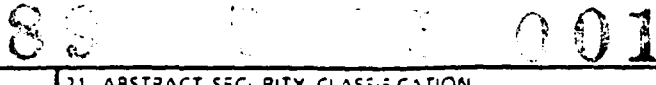


(2)

AD-A209 853

## REPORT DOCUMENTATION PAGE

Unclassified		1b. RESTRICTIVE MARKINGS	
2a. SECURITY CLASSIFICATION AUTHORITY		3. DISTRIBUTION/AVAILABILITY OF REPORT	
2b. DECLASSIFICATION/DOWNGRADING SCHEDULE		Approved for public release and sale. Distribution unlimited.	
4. PERFORMING ORGANIZATION REPORT NUMBER(S) ONR . Technical Report No. 6		5. MONITORING ORGANIZATION REPORT NUMBER(S)	
6a. NAME OF PERFORMING ORGANIZATION University of Wyoming	6b. OFFICE SYMBOL (If applicable)	7a. NAME OF MONITORING ORGANIZATION Office of Naval Research Resident Representative	
6c. ADDRESS (City, State, and ZIP Code) Département of Chemistry University of Wyoming Laramie, WY 82071-3838		7b. ADDRESS (City, State, and ZIP Code) University of New Mexico Bandelier Hall West Albuquerque, NM 87131	
8a. NAME OF FUNDING/SPONSORING ORGANIZATION Office of Naval Research	8b. OFFICE SYMBOL (If applicable) ONR	9. PROCUREMENT INSTRUMENT IDENTIFICATION NUMBER N00014-87-K-0674	
8c. ADDRESS (City, State, and ZIP Code) 800 N. Quincy Street Arlington, VA 2217		10. SOURCE OF FUNDING PROGRAM ELEMENT NO.	SERS TASK NO. R&T 413301901
		PROJECT NO.	WORK UNIT ACCESSION NO.
11. TITLE (Include Security Classification) Applications of the Quartz Crystal Microbalance to Electrochemistry			
12. PERSONAL AUTHOR(S) Daniel A. Buttry			
13a. TYPE OF REPORT Technical	13b. TIME COVERED FROM 9/88 TO 6/89	14. DATE OF REPORT (Year, Month, Day) 1989 June 29	15. PAGE COUNT 100
16. SUPPLEMENTARY NOTATION Prepared as a chapter for "Electroanalytical Chemistry. A Series of Advances." Marcel Dekker, ed. A. J. Bard			
17. COSATI CODES FIELD      GROUP      SUB-GROUP		18. SUBJECT TERMS (Continue on reverse if necessary and identify by block number) electrochemistry, quartz crystal microbalance, review	
19. ABSTRACT (Continue on reverse if necessary and identify by block number) An exhaustive review of the use of the QCM in studies of the electrochemical interface. The level is highly technical, being prepared for practicing electrochemists.			
 			
20. DISTRIBUTION/AVAILABILITY OF ABSTRACT <input checked="" type="checkbox"/> UNCLASSIFIED/UNLIMITED <input type="checkbox"/> SAME AS RPT <input type="checkbox"/> DTIC USERS		21. ABSTRACT SECURITY CLASSIFICATION Unclassified	
22a. NAME OF RESPONSIBLE INDIVIDUAL Daniel A. Buttry		22b. TELEPHONE (Include Area Code) (307) 766-6677	22c. OFFICE SYMBOL

**Applications of the Quartz Crystal Microbalance to Electrochemistry**

**Daniel A. Buttry  
Department of Chemistry  
University of Wyoming  
Laramie, WY 82071-3838**

prepared for publication in Electroanalytical Chemistry

## Table of Contents

I. Introduction	1
II. Experimental Methods	3
A. Instrumentation and Materials	3
B. Equivalent Circuit Description of the QCM	14
C. Effects of Various Parameters on Crystal	
Oscillation	17
D. Correlations between Frequency Changes and Electrochemical Parameters	30
III. Monolayer Systems	31
A. Introduction	31
B. Electrosorption of Oxides and Halides on Au	32
C. Underpotential Deposition of Metals	34
D. Adsorption/desorption of Surfactant	
Molecules	36
IV. Multilayer Deposition and Dissolution	39
A. Introduction	39
B. Deposition and Dissolution of Electrochromic Films of Diheptyliviogen Bromide	39
C. Other Systems	42
V. Polymer Films	43
A. Introduction	43
B. Redox Polymers	44
C. Conduction Polymers (Au)	49
VI. Future Applications of the EQCM	57

Accession For	
NTIS Serial	<input checked="" type="checkbox"/>
PTI Serial	<input type="checkbox"/>
Unpublished	<input type="checkbox"/>
Classification	
Physical Description	
Distribution	
Availability Codes	
Serial Number	
Date Received	
Date Entered	

A-1

## Applications of the Quartz Crystal Microbalance to Electrochemistry

Daniel A. Buttry

University of Wyoming

Laramie, Wyoming

### I. Introduction

The quartz crystal microbalance (QCM) is a piezoelectric device capable of extremely sensitive mass measurements. It oscillates in a mechanically resonant shear mode by application of an alternating, high frequency electric field using electrodes which are usually deposited on both sides of the disk. Sauerbrey was the first to recognize that these devices could be used to measure mass changes at the crystal surface (1). The mass sensitivity arises from a dependence of the oscillation frequency on the total mass of the (usually disk-shaped) crystal, its electrodes, and any materials present at the electrode surface. These devices have been used for many years to measure the masses of thin films in various types of deposition processes (2). To the extent that the density of the deposit is known, the thickness may be calculated, so these devices are used in a number of commercial film thickness monitors. Until about ten years ago it was thought that these crystals would not oscillate in liquids due to excessive energy loss to the solution from viscous effects. At that time Konash and Bastiaans (3) and Yamura (4) demonstrated the use of the QCM in the liquid environment for the determination of mass changes at the crystal surface. These reports made clear the potential utility of the QCM for accurate, in situ determinations of extremely small mass changes of the crystal electrodes or films deposited on them. Part I of this report includes:

The use of the QCM in an electrochemical context to monitor mass changes at

electrodes was first demonstrated by Jones and Mieure (5,6), who showed that trace metal determinations were possible by plating the metals onto a QCM electrode and measuring the change in resonant frequency of the crystal in air following its removal from the electrochemical cell. The first in situ application of the QCM to electrochemical problems was by Nomura and coworkers (7,8) who used it to determine Cu(II) and Ag(I) by electrodeposition. (Such in situ applications of the QCM to electrochemical systems will be distinguished from non-electrochemical applications by referring to the former as EQCM (electrochemical QCM) experiments.) When used as an in situ technique for measuring mass changes at electrode surfaces, one of the EQCM electrodes is used simultaneously to provide for the alternating electric field which drives the oscillation of the crystal and as the working electrode in the electrochemical cell. Thus, the EQCM experiment involves the measurement of the various electrochemical parameters, such as potential, current, and charge, at one of the EQCM electrodes and the simultaneous measurement of the oscillation frequency of the piezoelectric crystal from which, in favorable cases, minute mass changes at the electrode may be inferred. Various instrumental approaches to this have been used which will be described in a later section.

Since the pioneering publications of Nomura appeared the EQCM has been used to study monolayer and multilayer depositions and dissolutions, mass transport in polymer films on electrodes, corrosion processes at electrodes, electroless depositions, and mass changes caused by protein adsorption at electrodes. In addition, many other applications are on the horizon. It is the purpose of this Chapter to describe the use of the EQCM to study problems of interest to the electrochemical community, to give information about the experimental aspects of its in situ use, and to discuss its potential for future application. A detailed review of the piezoelectric effect in quartz crystals is not presented here, as this topic has been adequately discussed elsewhere (see reference 2 and references therein). Also, the use of the QCM for other (non-electrochemical) analytical applications

related to the determination of mass changes at surfaces in liquids or gases, while of considerable current interest, are not discussed in detail here, except to the extent that such results impact on electrochemical studies.

## II. Experimental Methods

### A. Instrumentation and Materials

#### 1. Crystals

Nearly all of the reported applications of the QCM have employed alpha quartz crystals because of the superior mechanical and piezoelectric properties of alpha quartz. The QCM transducers are prepared (usually by the manufacturer) by cutting the desired parts from large single crystals of alpha quartz at certain angles with respect to the crystalline axes of the quartz crystal (9). For QCM applications, the AT, BT, and SC (stress-compensated) cuts (9) have been most frequently employed. AT-cut crystals are particularly popular because they can be cut to give nearly zero temperature coefficients (the proportionality constant relating the oscillation frequency of a crystal in vacuum to its temperature) at one or two temperatures (9). However, as will be discussed below, temperature effects for crystals immersed in liquids far outweigh the intrinsic temperature dependence of the crystals themselves, and must be taken into account in most electrochemical applications. SC-cut crystals would seem to offer certain advantages in terms of the elimination of stress-induced frequency changes (*vide infra*), but have not as yet been investigated in EQCM applications. In the remainder of this Chapter, the discussion will be restricted to AT-cut crystals unless otherwise specified.

QCM crystals are typically employed as thin, disk-shaped transducers which oscillate in a pure shear mode when an alternating electric field of the proper frequency is applied across the disk, i.e. the electric field lines are normal to the disk surface. Figure 1 shows an edge view of a QCM disk with an exaggerated view of the shear distortion from the oscillation. The designation of the oscillation as a pure shear mode indicates that the

motion of the disk surface is precisely parallel to the disk face. Typical frequencies for these oscillations in EQCM's are from 1-10 megahertz (MHz).

Aside from the thickness shear mode described above, other modes of vibration can also be excited by the applied electric field. While most other modes are only weakly coupled to the shear mode, the flexural modes are sometimes strongly coupled (10). When the frequencies of these flexural modes are near that of the shear mode, deviations in resonant frequency can occur such that the response of the QCM to mass changes is no longer linear. Fortunately, it is usually possible to eliminate this source of error by proper design of the crystal and its electrodes. This will be described further below.

For shear mode oscillation, there are several frequencies which correspond to resonant conditions. The distinctions between these and their relevance will be described later. For the present purposes, the resonant frequency of the crystal may be identified as the frequency of maximum displacement of the crystal surface (for a constant driving voltage). This condition corresponds to the establishment of a standing acoustic wave within the bulk of the crystal with a node existing in the center of the disk (see Figure 1) and the antinodes at the two surfaces. The resonant frequency can thus be seen to be related to the thickness of the crystal through the following equation:

$$t_q = v_q/2f_0 = \lambda_q/2 \quad (1)$$

where  $v_q$  is the velocity of the acoustic wave in quartz,  $f_0$  is the resonant frequency,  $t_q$  is the thickness, and  $\lambda_q$  is the wavelength of the acoustic wave in quartz. This equation shows the reciprocal dependence of  $f_0$  on the crystal thickness. For an AT-cut crystal  $v_q = 3340 \text{ m s}^{-1}$  (11) which gives  $t_q = 334 \mu\text{m}$  and  $\lambda_q = 668 \mu\text{m}$  for a crystal with a resonant frequency of 5 MHz. Higher frequency, odd harmonics may also be excited. These will be considered further below in regards to the higher mass sensitivity obtained at these higher frequencies.

Figure 2 shows a top view of a QCM disk with electrodes in what is sometimes called

a keyhole pattern. The crystals used in these laboratories are one inch in diameter, with a concentric disk electrode of area  $0.28 \text{ cm}^2$ . Smaller diameter crystals may also be used (12). Small crystals have the advantage of being less expensive, but they suffer from the serious drawback that the structures used to mount the crystal are closer to the piezoelectrically active area, so the influence of stress from the mounting can become a problem (13). Larger crystals allow for the mounting structures to be farther from the region of the crystal undergoing displacement (which is nearly confined to that part of the crystal sandwiched between the two circular pads in the center of the disk (1,14)).

As stated above, the dimensions of the electrodes and the crystal disk have a strong influence on the coupling of other modes to the thickness shear mode. This coupling represents a source of spurious frequency changes which must be addressed for optimum performance of the EQCM. A recent discussion of the frequency, amplitude, and shape of vibrations in quartz crystals describes many of the design criteria which provide for the suppression of unwanted modes (15). The critical dimensions are the thickness of the quartz disk ( $t_q$ ), the diameter of the crystal ( $d_c$ ), and the diameter of the concentric electrode pad ( $d_e$ ). For a ratio of  $d_c/t_q$  of greater than 50, unwanted modes may be suppressed by 40 dB when the ratio of  $d_e/t_q$  is larger than 18 (15). The values of these ratios for the design in Figure 2 are 85 and 20, respectively, well within the acceptable ranges for excitation of the thickness shear mode without significant coupling to other modes. Following these design criteria, the minimum value of  $d_c$  for a 5 MHz crystal ( $t_q = 3 \times 10^{-2} \text{ cm}$ ) is 1.5 cm, and the minimum value for  $d_e$  is 0.54 cm. These calculations do not take into consideration the "flag" which extends from the edge of the circular part of the electrode to the edge of the crystal disk, but it has generally been found that the flag has minimal influence on oscillator stability.

Another way of considering the problems of coupling to unwanted modes or to the structures used to mount the crystal is with the concept of energy trapping (9,15). Energy

trapping refers to the fact that most of the energy contained in the mechanical oscillation of the crystal can be confined to the electroded region of the crystal if this region has a resonant frequency which is significantly lower than that of the non-electroded region. This can be easily effected by using rather thick electrodes (with thicknesses greater than, say, 100 nm) or by contouring one or both faces of the crystal disk so that the thickness of the electroded region is significantly different than that of the rest of the disk (9).

The two predominant types of AT-cut crystals used for mass measurements are the so-called plane and the plano-convex. Plane crystals have both disk surfaces parallel to within ca. 1  $\mu\text{m}$ , depending on the manufacturer. Plano-convex crystals have one side of the disk flat and the other ground to have a very slight radius of curvature. A typical range of radius of curvature for a 1 inch diameter, 5 MHz crystal would be 10-50 cm. For plano-convex crystals the region of the crystal which undergoes displacement during the oscillation (and therefore senses mass changes) is confined completely to the area defined by the electrodes (or by the smaller of the two electrodes if they have different sizes) (13). For plane crystals this region extends somewhat past the edge of the electrode, onto the face of the quartz disk itself (1,13,15). The degree of extension of this region depends on the total mass loading of the crystal, with the displacement being more completely confined to that part of the crystal sandwiched between the electrodes for higher loading. The amplitude of the displacement is known to depend on the driving voltage (15), and probably also depends on the total mass loading. For AT-cut crystals operating in the frequency range of 1-10 MHz in the fundamental mode, the range of amplitudes reported is from ca. 10 to 100 nm, as determined by a wide variety of optical methods as well as electron microscopy (1,15,16). These are fairly large displacements with respect to molecular dimensions, but it should be kept in mind that the relative velocities and displacements of the electrode surface with respect to the solution are much smaller. This is because the boundary layer of solution very near to the surface is dragged along with the

surface at a similar velocity.

The distribution of the vibrational amplitude as a function of radial distance from the center of the electrode is also known from the same studies (15-17). The amplitude is maximum in the center of the disk and decays in an apparently Gaussian fashion with distance, nearly reaching zero at the edge of the electrode. This Gaussian distribution becomes considerably sharper for plano-convex crystals as the radius of curvature is decreased or with increasing harmonic number. For example, for a 4 MHz crystal operating in the fundamental mode, the radial distance at which the amplitude is 1/e of its maximum value decreases by 30% when the radius of curvature is decreased from 50 to 6 cm (16). Also, for a crystal having a radius of curvature of 10 cm, this distance is decreased by 50% when the crystal is operated in its 3rd harmonic mode (12 MHz) as opposed to the fundamental mode (4 MHz) (16). Thus, for plano-convex crystals or for plane crystals operated in the 3rd harmonic, the vibrational amplitude can be considered to be essentially zero at the edge of the electrode. For plane crystals operated in the fundamental mode in vacuum or in a low density gaseous environment, the amplitude distribution is known to be more confined to the electrode area as mass loading is increased (13).

Since the mass measurement made with quartz resonators is actually an inertial measurement, the mass sensitivity is intimately related to the vibrational amplitude distribution. There is ample experimental evidence supporting a Gaussian mass sensitivity for AT-cut crystals (1,13,15-19) with the maximum sensitivity at the center of the electrode and zero sensitivity at the edges for plano-convex or harmonically driven plane crystals. In one particularly revealing study, the mass sensitivity distribution for plane crystals was shown to become slightly more confined to the electrode region as the mass loading was increased (13). The differential mass sensitivity,  $c_f = df/dm$ , was shown to be a function of radial distance from the center, while the integrated mass sensitivity,  $C_f$ , given

by equation 2, was shown to change slightly at small loadings and then become relatively constant for larger loadings (1,15-20):

$$C_f = \int c_f dA \quad (2)$$

where A is the area of the vibrational displacement.

The implication of this differential radial mass sensitivity for EQCM applications is that the distribution of any mass changes at the electrode surface must be known, whether or not it is uniform. That the radial mass sensitivity changes with mass loading might at first glance seem to cause problems (i.e. a different proportionality constant relating frequency and mass for different mass loadings). However, the evidence is that most of the change occurs at fairly low mass loadings, with little change in the radial mass sensitivity at higher loadings (13,19,20). Thus, since the mass loading from the vapor deposited electrodes and from immersion of the crystal in a liquid is so large, it would seem that this alone would serve the function of keeping the vibration amplitude confined to the electrode region, thereby bringing the value of  $C_f$  to its high-loading limit. This is an important consideration for precise, *in situ* mass measurements with these devices which has not yet been addressed experimentally.

A thin (ca. 2-5 nm) adhesion layer of either Cr or Si is usually deposited directly onto the quartz crystal to aid in the adhesion of the metal electrode. Spurious electrochemical responses can sometimes result if diffusion of the material from the adhesion layer to the electrode surface occurs. Au electrodes have been the most commonly used in EQCM studies because of the ease with which Au is evaporated. However, Cu, Pt, Ni, and other metals have also been employed. In principle, any type of material which can be deposited onto the surface of the underlying metal electrode, either by electrodeposition or from vacuum, can be used. The only limitations on the use of such materials are that they have good adhesion to the underlying electrode (which must be present to supply the alternating electric field) and the deposition must be carried out in such a way that the temperature of

the quartz crystal does not exceed 573 °C, above which alpha quartz loses its piezoelectric activity (21). It is worth pointing out here that mass changes at the EQCM electrodes influence  $f_0$  because these electrodes actually become a part of the composite resonator composed of the quartz crystal, its electrodes, any film deposited on the electrodes, and any liquid adjacent to the electrode (or deposit) surface which experiences shear forces. Thus, when the electrodes become delaminated due to poor adhesion of the underlayer, large, discontinuous changes in frequency occur which render a particular crystal useless.

Considering both convenience and cost, it is nearly essential that crystals be reused, i.e. cleaned and recoated with fresh electrodes when a particular experiment is over. This can be done if facilities for vacuum deposition are available. Either thermal or sputtering techniques may be employed. To ensure reproducible results careful attention to cleanliness must be paid, both in the vacuum chamber and in the preparation of the crystal blanks prior to deposition. Normal methods for cleaning glass parts may be used with the exception of basic baths which will cause etching.

Crystals may be obtained with either rough or smooth surfaces. Rough surfaces are the most common because they are less expensive, but they suffer from a quantitatively unpredictable dependence of the absolute oscillation frequency in a liquid on the trapping of the liquid in the pores on the surface (22,23). The influence of surface roughness and deposit morphology on the oscillation frequency will be discussed further below. Crystals having smooth surfaces are sometimes called overtone polished crystals because the excitation of overtone (harmonic) modes requires a flatter surface due to the smaller wavelength of the acoustic wave at higher frequencies. This type of crystal is generally preferred because roughness effects then exist only in the deposit (which might be of interest, depending on the system studied) and do not arise from the underlying electrodes.

As stated above, EQCM's may be operated either in the fundamental mode or in any of the higher frequency, odd harmonics. The advantage of higher frequency operation is a

greater mass sensitivity. However, since  $f_0$  is inversely related to  $t_q$  it becomes increasingly difficult to handle the extremely thin crystals which are needed for high frequency operation in the fundamental mode. Thus, a practical limit of about 15 MHz exists for the fundamental frequency of crystals which can be easily handled. Note that a 15 MHz crystal is just slightly thicker than 100  $\mu\text{m}$ . Use of lower frequency crystals at odd harmonics is possible (24) at the expense of slightly more complicated oscillator circuitry. Another potential difficulty with the use of higher frequencies is that the viscous damping from the solution can more easily cause the oscillation to cease, depending on the circuitry used. A common cause of this would be roll-off in the gain of the oscillator circuit at the higher frequency. A good compromise used in these laboratories is the use of 5 MHz crystals which offer acceptable (submonolayer) mass sensitivity, relative robustness, and stable oscillation in most viscous media (given the proper oscillation circuitry).

## 2. Cells

The method of mounting the crystals to the electrochemical cell is an important consideration because of possible influences of stress on the absolute frequency of oscillation, either in air or liquid, and because simple and rapid exchange of crystals is required when the thin film electrodes become damaged (which can occur from large potential excursions, aggressive chemical treatments, or mechanical abrasion). Several methods for mounting have been described (12,25-29), all of which make it possible to expose only one side of the EQCM disk (the working electrode side) to the electrolyte solution. This is usually necessary to prevent the two EQCM electrodes from being capacitively shunted by the solution, which can cause the cessation of oscillation (12). It is possible to ~~safely~~ attach the crystals to an opening on the cell with some type of adhesive (12). However, this method does not provide for easy replacement of the crystal when damage occurs. Another method which allows the use of glass cells is to sandwich the crystal between two o-rings in a vacuum o-ring joint which has been blown onto a

standard H-cell (26). In these laboratories a number 9 o-ring joint is used with the material of the o-ring chosen for compatibility with the solvent system under investigation. Finally, cells of Kel-F, Teflon, or other chemically inert materials can be employed with mounting again achieved by sandwiching between o-rings (25,27-29). Large diameter crystals and o-rings seem to be best for keeping the mounting stresses away from the piezoelectrically active area. In all cases, the cells should be designed so that the oscillator circuitry is situated as close as possible to the crystal to minimize the length of the leads from the circuit to the crystal.

### 3. Oscillator circuits

The oscillator circuit used determines in large measure the stability of the instrument and, therefore, the types of experiments which can be done. A key requirement of the circuit is that it provide sufficient gain to allow for oscillation of the crystal in a viscous medium. Three different designs have thus far been reported (12,24,25). In one of the designs, the oscillation frequency of the EQCM crystal is measured with respect to a reference crystal which is external to the electrochemical cell (12). Depending on the configuration used, the output can be sent to a frequency-to-voltage converter or a frequency counter. This design has the advantage of not requiring the use of a frequency counter. A disadvantage of this design would seem to be its failure to use a true ground for the EQCM working electrode. However, this system has been used to produce data on monolayer mass changes (perhaps the most challenging application for EQCM instrumentation) with very good signal to noise ratios. The second design (25) uses a modified Pierce-Miller oscillator with a high frequency 2N1711 transistor operating as an inverting amplifier. This is a more conventional design, similar to those used in many types of frequency control oscillator circuits (30). The EQCM working electrode is at true ground, facilitating the connection of electrochemical circuitry, and some adjustment is provided to increase signal amplitude when viscous losses are severe.

Figure 3 shows the oscillator circuit used in the author's laboratory. This is essentially the same as that designed by Kanazawa (24), but it lacks the inductor-capacitor (LC) tuned element used to provide for oscillation at the third harmonic. This oscillator uses a Motorola MC1733 differential video amplifier as the central component, with a 2N3904 switching transistor in the feedback loop to provide for the signal inversion needed to achieve oscillation. The MC1733 is strapped for maximum gain (x400) and the transistor also provides significant gain (x50-200). The Schottky diodes act as limiters to prevent the crystal from damage due to large driving voltages. The values of the resistors in the feedback loop were chosen to provide for maximum stability of the oscillation frequency under conditions of viscous loading. The other output of the differential amplifier is sent to a frequency counter, which will be described below. A significant attribute of this circuit is that it provides a relatively constant ac voltage across the crystal (ca. 0.4 V peak to peak with a power supply voltage of 3.5 V) for a wide range of viscous loading conditions. This will be true so long as the gain is large enough for the diode limiters to be the elements determining the voltage in the feedback loop. Thus, the circuit is usually able to sustain crystal oscillation even under conditions of large viscous loading from thick, viscoelastic polymer films and highly viscous solutions. Most importantly, changes in this viscous loading do not appear to have strong influence on the characteristics of the oscillator circuit. In addition, the EQCM working electrode is at true ground which conveniently allows the use of Wenking-style potentiostats. Several groups have reported the successful use of this circuit (24,26,29,31-33).

#### 4. EQCM apparatus

Figure 4 shows a schematic of the EQCM instrument used in the author's laboratory. The quartz crystal is mounted in the electrochemical cell with one electrode exposed. This electrode is maintained at true ground and is connected to the ground of the oscillator circuit and to the working electrode lead of the Wenking style potentiostat previously

described (24). The other crystal electrode is connected to the "hot" side of the oscillator circuit. These connections are made using small, flat-nosed alligator clips. Silver paint is used on the electrode flags to protect the thin Au films from abrasion. The oscillator circuit is connected to the frequency counter, which generates either an analog (0 to 1 V) or digital (IEEE 488) signal for the computer acquisition system. The frequency counter used in these laboratories is a Philips PM 6654, capable of measuring frequencies with an accuracy of 1 part in  $10^6$  in as little as 6 msec. Many commercial counters would require 1 second for such a measurement. Since the rapidity of the frequency measurement is generally the factor which limits the time scale of the experiment, it is desirable to use a counter with the maximum counting rate available. Connection to the computer (an IBM PC, AT, or 80386-based clone) is made with an A/D board such as the Data-Translation DT 2801-A or using any of a number of IEEE 488 boards. The Philips PM 6654 provides for either type of connection with accessory plug-in boards.

The potentiostat is of the standard Wenking design, using a true ground for the working electrode. Potentiostatic or galvanostatic control is achieved either by using the DT 2801-A to generate staircase waveforms or by triggering an external analog ramp generator. In the absence of an external analog ramp generator, the 12 bit accuracy of the DT 2801-A forces the use of staircase voltammetry because the resolution is not sufficient to produce a staircase waveform which mimics closely enough the analog ramp required for cyclic voltammetric experiments.

With the instrument shown in Figure 4, a typical cyclic voltammetric EQCM experiment would involve the application of the electrochemical waveform to the working electrode and (virtually) simultaneous measurement of the current flowing through the electrochemical cell and the oscillation frequency of the crystal. For large currents ( $i > 1\mu A$ ) or large frequency changes ( $\Delta f > 10\text{Hz}$ ), single scans are generally sufficient to achieve acceptable signal to noise ratios. Smaller signals require the use of signal

averaging techniques. As always, proper attention to shielding is required for achieving the maximum signal to noise ratio (34). Placing the oscillator circuit within a shielded metal enclosure has been found to be especially helpful in reducing noise levels.

A variation on the apparatus shown in Figure 4 is one in which the oscillator and frequency counter are replaced by some type of impedance analyzer or network analyzer. The use of such instruments in EQCM applications has not yet been described in the literature. However, experiments in these laboratories have shown it to be a useful complement to the more standard configuration of Figure 4. The parameters which can be measured using such instruments and their relevance to the EQCM experiment are discussed below. Again, it is especially useful if one of the inputs to the impedance analyzer can be maintained at true ground. A Hewlett-Packard 4192A low frequency impedance analyzer is used in these laboratories for this reason.

#### B. Equivalent circuit description of the EQCM

The equivalent circuit description of the quartz crystal has been widely used to model its behavior in oscillator circuits (9,30). Figure 5a shows the equivalent circuit for an AT-cut crystal. Figure 5b shows an equivalent representation of this circuit which is of some use in the experimental determination of the values of the circuit elements in Figure 5a. In Figure 5a,  $C_0$  is the electrical capacitance of the quartz sandwiched between the two vapor deposited electrodes,  $R_1$  corresponds to the dissipation of the oscillation energy from mounting structures and from the medium surrounding the crystal (e.g. losses induced by the presence of a viscous solution),  $C_1$  corresponds to the stored energy in the oscillation and is related to the elasticity of the crystal and the surrounding medium, and  $L_1$  corresponds to the inertial component of the oscillation which is related to the mass displaced during the vibration. In Figure 5b,  $R_e$  and  $X_e$  represent the resistive and reactive components of the circuit in Figure 5a, respectively (30). Typical values for the components in Figure 5a at the fundamental frequency of the crystals shown in Figure 2

are  $C_0 = 7.3 \times 10^{-12} \text{ F}$ ,  $R_1 = 100 \Omega$ ,  $C_1 = 23 \times 10^{-15} \text{ F}$ , and  $L_1 = 45 \times 10^{-3} \text{ H}$ . These values are those found for a crystal with both faces exposed to air. The values are different for crystals operated at their harmonic frequencies.

For a crystal with one face exposed to an aqueous solution, the value of  $R_1$  increases to ca. 500-1500  $\Omega$  depending on the solution, with little change in the other values, confirming the notion that  $R_1$  can be associated with the viscous loading introduced by immersion of the crystal in the solution. The determination of  $R_1$ , which will be discussed below, thus provides a means of evaluating the extent of changes in viscous loss due to changes in the surrounding medium.

Several workers have analyzed the circuit in Figure 5a, providing expressions for the various resonant frequencies and a few other parameters of interest (9,30). The frequency of maximum conductance,  $f_s$ , is the resonant frequency of the motional branch of the circuit, where the conductance,  $G$ , (i.e. the real part of the admittance) is a strong function of the applied frequency near the resonant point. The frequency of zero phase,  $f_r$ , occurs when the current flowing through the crystal is exactly in phase with the applied voltage. The sharpness of the resonance is measured by the  $Q$  value or quality factor of the resonator. Another parameter of interest is the capacitance ratio,  $r$ . Equations 3-6 give some relevant relationships between these variables:

$$f_s = \{2\pi(L_1 C_1)^{1/2}\}^{-1} \quad (3)$$

$$Q = (2\pi f_s C_1 R_1)^{-1} = 2\pi f_s L_1 / R_1 \quad (4)$$

$$(f_r - f_s)/f_s = r / (2Q^2) \quad (5)$$

$$r = C_0 / C_1 \quad (6)$$

Note that  $f_s$  and  $f_r$  are, in general, not equal, and that their separation depends on both  $r$  and  $Q$ .

Experimentally, one approach to obtaining these values is to measure the appropriate combinations of functions using an impedance analyzer, network analyzer, or bridge

methods. A Hewlett-Packard 4192A impedance analyzer is used for this purpose in these laboratories. This type of instrument performs an essentially different function than does the apparatus shown in Figure 4 above. An alternating voltage having a precise, synthesized frequency is applied to the crystal, usually with the capability of sweeping this frequency over a wide range. The amplitude and phase of the ac current which passes through the crystal are measured, and these quantities are used to compute various parameters of interest. Such measurements directly provide the conductance ( $G$ ), the reactance ( $X_e$ ), the resistance ( $R_e$ ), and the phase angle ( $\Theta$ ), as well as several other parameters which are characteristic of the crystal resonator. Note that  $G$ ,  $X_e$ ,  $R_e$ , and  $\Theta$  are functions of frequency, and in general vary strongly near the resonant point.  $f_r$  is obtained from the frequency at which  $\Theta = 0^\circ$ .  $f_s$  is found from the frequency at which  $G$  is a maximum (i.e.  $G = G_{\max}$ ).  $R_1$  is approximately equal to  $R_e$  at the frequency at which  $X_e$  is equal to zero, which is just above  $f_s$  (30).  $C_0$  may be measured at any frequency sufficiently far from the resonant frequency of the motional branch of the circuit (e.g. 100 kHz). Thus, the measured quantities are  $R_1$ ,  $C_0$ ,  $f_r$ , and  $f_s$ . Equation 7, obtained by combination of equations 4-6, gives  $C_1$  as a function of these known quantities:

$$C_1 = (f_r - f_s) (2\pi^2 f_s^3 C_0 R_1^2)^{-1} \quad (7)$$

Once  $C_1$  is known,  $L_1$  may be calculated from equation 3 and  $Q$  from equation 4 or 5.

A dimensionless quantity which is frequently referred to in discussions of quartz crystal oscillators is the figure of merit,  $M = Q / r$ . It has been shown (9) that when  $M < 2$  then  $f_r$  will not exist, i.e. there will be no frequency at which the zero phase condition exists. For typical AT-cut crystals operating at 5 MHz, this will occur when  $R_1$  exceeds ca. 3000  $\Omega$ . Since most oscillator circuits actually operate at a zero phase condition (which may not occur at exactly the same frequency as  $f_r$  due to influence of the components of the oscillator circuit), there will usually be cessation of oscillation when excessive viscous loss causes  $R_1$  to be larger than this value. Values of  $R_1$  in excess of this are rather easily

obtained when thick, solvent-swollen polymer films are investigated with the EQCM. However, even under these conditions it is still possible to make meaningful measurements of crystal parameters (e.g. to monitor changes in  $G_{max}$  as mass loading changes) if an impedance analyzer is available.

The purpose of this section has been to briefly describe the use of impedance analysis methods for the evaluation of some of the important parameters which can be used to judge the type of behavior exhibited by a particular QCM composite resonator (i.e. the quartz, electrode, thin film, solution system). In the sections below the criteria for such judgements are discussed, with emphasis on the ability to distinguish between rigid, elastic, and viscoelastic behavior. As will be seen, such distinctions are crucial to the proper application of the EQCM to quantitative mass measurements.

### C. Effects of various parameters on crystal oscillation

#### 1. Mass-frequency correlations

Sauerbrey was the first to recognize the potential usefulness of AT and BT crystals as mass sensors (1). He demonstrated the extremely sensitive nature of these piezoelectric devices towards mass changes at the surface of the QCM electrodes. He also described their differential radial mass sensitivity and correlated this with the radial distribution of the vibrational amplitude (17). The results of his pioneering work in this area are embodied in the Sauerbrey equation, equation 8, which relates the mass change at the QCM electrode surface to the observed change in oscillation frequency of the crystal:

$$\begin{aligned}
 \Delta f &= - (f_0 / t_q \rho_q) \Delta m \\
 &= - (2 \pi f_0^2 / (\rho_q \mu_q)^{1/2}) \Delta m \\
 &= - (f_0^2 / N \rho_q) \Delta m \\
 &= - C_f \Delta m
 \end{aligned} \tag{8}$$

where  $\Delta f$  is the observed frequency change (Hz),  $f_0$  is the resonant frequency of the fundamental mode of the crystal (which may be significantly different than either  $f_s$  or  $f_r$ ,

depending on the particular oscillator circuit used),  $\Delta m$  is the change in mass per unit area ( $\text{g cm}^{-2}$ ),  $\rho_q$  ( $= 2.648 \text{ g cm}^{-3}$ ) is the density of quartz,  $\mu_q$  ( $= 2.947 \times 10^{11} \text{ g cm}^{-1} \text{ s}^{-2}$ ) is the shear modulus of quartz,  $N$  ( $= 1670 \text{ kHz mm}$ ) is the frequency constant for quartz,  $n$  is the number of the harmonic at which the crystal is being driven (i.e. 1 for the fundamental, 3 for the third harmonic, etc.) and  $C_f$  is the sensitivity factor for the crystal employed for the measurement, which depends on the thickness, and therefore, the fundamental frequency. For a 5 MHz crystal operated in its fundamental mode,  $C_f$  is  $56.6 \text{ Hz } \mu\text{g}^{-1} \text{ cm}^2$ , so that a uniformly distributed mass increase of  $1 \mu\text{g cm}^{-2}$  would result in a frequency decrease of 56.6 Hz. The sensitivity factor is a fundamental property of the QCM crystal. Thus, these mass sensors do not require calibration. This ability to calculate the mass sensitivity from first principles is a most attractive feature of these devices.

Equation 8 shows the linear dependence of  $\Delta f$  on  $\Delta m$ , the dependence of  $\Delta f$  on  $f_0^{-2}$ , and the linear increase in sensitivity which accompanies the use of higher harmonics (i.e.  $\Delta f \propto n$ ). Thus, for a given crystal, the mass sensitivity increases linearly with the harmonic number, while for different crystals, the mass sensitivity increases as the square of the fundamental frequency. The implication of this is that sensitivity enhancements need not be made through the use of crystals with high fundamental frequencies (which are necessarily thin and fragile). Rather, such enhancements may be made by driving crystals having lower fundamental frequencies at their harmonics. This occurs at the expense of greater complexity in the oscillator circuitry.

The negative sign shows that increases in mass correspond to decreases in frequency. The rather strong functional dependence of the mass sensitivity on  $f_0$  dictates that for precise work the deviation of the fundamental frequency from the nominal value must be taken into account. In other words, in the example above  $C_f$  would need to be modified appropriately if  $f_0$  were much different from 5 MHz (e.g. 4.9 rather than 5 MHz).

Equation 8 is indirectly based on equation 1 in that the incremental change in mass

from the foreign film is treated as though it were really an extension of the thickness of the underlying quartz disk. Thus, the material properties of the foreign film are not considered explicitly in equation 8. The foreign film is considered to be so thin that it exists entirely at the antinode of the vibration, so that it does not experience any shear forces. When this implicit assumption does not hold true, then the material properties of the foreign film must be taken into account.

Sauerbrey's early work has been extensively discussed and extended (see reference 2 and references therein). Significant improvements in later treatments have centered around the explicit incorporation of the elasticity (i.e. the shear modulus) of the deposit (35,36) and the extension of the measurement to higher harmonics (37). Lu and Lewis (36) gave an especially simple equation for the dependence of  $\Delta f$  on  $\Delta m$ :

$$\tan(\pi f_C/f_0) = - (z_f/z_q) \tan(\pi f_C/f_f) \quad (9)$$

where  $f_C$  is the resonant frequency of the composite resonator formed from the crystal and the film(s) present at the surface,  $f_f$  can be thought of as the resonant frequency of the free standing foreign film, and  $z_f$  and  $z_q$  are the acoustic impedances of the film and quartz, respectively. Equation 8 can be shown to be an approximation of equation 9 in which the tangent function is expanded in a power series, retaining only the first term. Some equations which interrelate these parameters are:

$$\Delta f = f_C - f_0 \quad (10)$$

$$f_f = v_f / 2 t_f = v_f \rho_f / 2 \Delta m \quad (11)$$

$$v_f = (\mu_f / \rho_f)^{1/2} \quad (12)$$

$$v_q = (\mu_q / \rho_q)^{1/2} \quad (13)$$

$$z_q = \rho_q v_q = (\rho_q \mu_q)^{1/2} \quad (14)$$

$$z_f = \rho_f v_f = (\rho_f \mu_f)^{1/2} \quad (15)$$

where  $t_f (= \Delta m / \rho_f)$  is the film thickness,  $\mu_q (= 2.947 \times 10^{11} \text{ g cm}^{-1} \text{ s}^{-2})$  and  $\mu_f$  are the shear moduli of quartz and film, respectively,  $\rho_f$  is the density of the film, and  $v_q$  and  $v_f$

are the velocities of the acoustic waves in the quartz and film, respectively. This analysis of frequency changes using the acoustic impedances of the quartz and film is usually called the Z-match method.

The choice of whether to use equation 8 or 9 for determining the mass change for deposition or dissolution processes of rigid films at electrode surfaces depends on the thickness of the deposit which is to be investigated. (Considerations pertaining to non-rigid films will be discussed below.) When the mass loading from the deposit causes a change in the resonant frequency of less than 2% of  $f_0$ , then equation 8 may be used. Equation 9 is accurate for frequency changes of up to ca. 40% of  $f_0$  (36). The degree to which equation 8 deviates from the more accurate equation 9 depends on the ratio of acoustic impedances for quartz and the deposit.

Use of the Z-match method requires that the shear modulus of the deposit be known. While this will not be a problem for many cases (e.g. some metal or metal oxide bulk depositions), in other instances the properties of the deposit may be completely unknown or may be very different from those of the bulk material. It has been asserted that the density of solid materials varies more strongly than does the shear modulus from one material to another (37). Thus, an approximation for the  $z$  of a deposit may be obtained (if its density is known) by assuming that its shear modulus is the same as that of quartz (i.e.  $z_f, \text{approx} = (\rho_f \mu_q)^{1/2}$ ). However, this provides only a very rough approximation of  $z_f$ , and still requires that  $\rho_f$  be known.

An alternative method (37) makes use of the fact that the response of the crystal to varying acoustic impedance of the foreign film is different at the fundamental and harmonic frequencies. Measurement of the change in resonant frequency at more than one frequency (usually the fundamental and third harmonic) thus provides a method for obtaining  $z_f$ , allowing the use of equation 9 for the accurate calculation of mass changes. This method will be useful only when the relative frequency change is large (greater than

ca. 10%), because this is the condition required for significant deviation from equation 8. Experimentally, this method requires the use of an oscillator that can be easily switched between operation at the fundamental and third harmonic frequencies or the use of an impedance analyzer which can operate at a frequency high enough to measure the parameters of interest at the third harmonic. Details of the method have been described (37).

Even though the influence of the deposit elasticity on the frequency change can be easily dealt with, it will frequently be true that equation 8 provides sufficient accuracy, because the film thickness (and, therefore, the relative frequency change) will be small. However, this situation holds only for rigid deposits. Films which are behaving viscoelastically, such as some organic polymer films with large thickness or viscosity, will exhibit significant deviations from both equations 8 and 9. The influence of such effects is discussed below.

## 2. Effect of the solution on oscillation

When a planar surface which is oscillating in a shear mode is immersed into any medium, a shear wave propagates normally away from the surface into the medium. Because of the energy dissipation caused by the viscous response of liquids, the shear wave is damped exponentially as it travels through the liquid away from the surface. This situation, as applied to oscillating quartz AT shear wave transducers, was first treated by Glassford (38) and later by Kanazawa and Gordon (39,40). The equation for the shear wave velocity as a function of distance from the surface of the oscillating crystal was given (39):

$$v(z,t) = v_0 \exp(-k_1 z) \cos(k_1 z - 2\pi f_0 t) \quad (16)$$

where  $v(z,t)$  is the shear velocity (parallel to the surface) which is a function of distance ( $z$ ) from the surface (which is at  $z=0$ ) and time ( $t$ ),  $v_0$  is the velocity of the crystal surface,  $k_1$  is the propagation constant, and the other quantities have been defined. The propagation

constant  $k_l$  is given by:

$$k_l = (\pi f_0 \rho_l / \eta_l)^{1/2} \quad (17)$$

where  $\rho_l$  and  $\eta_l$  are the density and viscosity of the liquid, respectively. Equation 16 shows the damped sinusoidal nature of the shear wave, and equation 17 shows the dependence of the damping on the density and viscosity of the medium. Figure 6 (40) shows the shear velocity profiles in the fluid at three different times: at peak surface velocity, at intermediate surface velocity, and at zero surface velocity.

The reciprocal of the propagation constant is the decay length of the shear wave. For pure water at 20 °C, with  $\rho_l = 0.9982 \text{ g cm}^{-3}$  and  $\eta_l = 1.002 \times 10^{-2} \text{ g cm}^{-1} \text{ s}^{-1}$ , this length is ca. 250 nm. Thus, only the first micron or so of the solution is perturbed by the shear displacement. Since these displacements are parallel to the surface and rather small (10-100 nm, see above), there should be negligible stirring effects, as has been found by workers in these laboratories and others.

Kanazawa's treatment of the influence of the solution properties on the crystal permits the prediction of the change in resonant frequency which accompanies immersion of the crystal into a viscous medium. This is given in equation 18:

$$\Delta f = - f_0^{3/2} (\rho_l \eta_l / \pi \rho_q \mu_q)^{1/2} \quad (18)$$

where the decrease in resonant frequency is seen to be proportional to  $(\rho_l \eta_l)^{1/2}$ . This equation predicts a decrease in  $f_0$  of ca. 700 Hz on transfer from vacuum to pure water at 20 °C. Due to experimental difficulties associated with mounting stresses, it has been more common to measure frequency changes for different solutions relative to pure water. Very good agreement with equation 18 for such relative changes has been obtained for aqueous solutions of glucose, sucrose, and ethanol using this type of differential measurement (39,40). Linearity to only the solution viscosity has also been demonstrated (12), indicating that density effects can be neglected under certain conditions, but this will not be true in general.

Based on the results of an analysis similar to Kanazawa's, Hager has proposed that the QCM can be used in the evaluation of fluid properties, specifically  $(\rho_l \eta_l)^{1/2}$  (41). A significant result of this contribution was the demonstration that the Gaussian velocity distribution of fluid at the crystal surface can be replaced by a surface average velocity, making the analysis of the problem considerably more tractable. He also proposed the use of multiple crystal arrays for the separate determination of  $\rho_l$  and  $\eta_l$  from the frequency shifts caused by exposure of the crystals to a fluid.

In a recent contribution, the equivalent circuit description of the QCM has been used to derive an equation relating  $R_1$  to  $(\rho_l \eta_l)^{1/2}$  (42). Impedance analysis techniques were used to arrive at a value of  $R_1$ , and this was plotted versus  $(\rho_l \eta_l)^{1/2}$  for water/ethanol and water/glycerol mixtures. Good linearity was observed except for the case of crystals which had both electrodes immersed in solutions with high proportions of water. This deviation was rather speculatively attributed to unusual dielectric properties of water or to unknown electrical effects. However, the important finding was the linearity of  $R_1$  to  $(\rho_l \eta_l)^{1/2}$ . Thus,  $R_1$  serves as a good measure of viscous loading by the medium at the crystal surface.

When the EQCM resonator is loaded by viscous coupling to a liquid, its conductance spectrum exhibits predictable changes. Recalling equation 4, which shows the reciprocal dependence of the crystal Q on the value of  $R_1$ , it is predicted that the increase in viscous loss should appear as an increase in  $R_1$ , and therefore, as a decrease in Q. The methods described in Section B above may be used to measure the changes in  $R_1$ .

A more intuitive, graphical way of measuring the changes in viscous loading is provided by plots of conductance (the real part of the admittance) versus frequency, which can be conveniently obtained using impedance or network analyzers. Figure 7 shows such a plot for a 5 MHz crystal, mounted in the o-ring mounting as in Figure 4, both in air (curve A) and in water (curve B) at room temperature. Curve A shows the sharpness of the

resonance when viscous loading is absent, while curve B (note the difference in vertical scales for the two curves) shows the dramatic increase in the width of the resonance and decrease in the maximum conductance which accompany immersion in the liquid. The size of the frequency shift, ca. 800 Hz, is in reasonable agreement with the prediction from equation 18 (700 Hz). A measure of the change in  $Q$  is obtained graphically by comparison of the widths at half height for these conductance plots. In this way, the  $Q$  is found to decrease by a factor of ca. 15 upon immersion of the crystal in water. As will be discussed below, the changes in  $Q$  induced by changes in the viscoelastic properties of the deposit may also be monitored by such impedance techniques.

The dependence of  $f_0$  on the properties of the liquid at the crystal surface has important consequences for experiments in which transfer from one solution to another is needed (e.g. in measuring changes in swelling for polymer films in different solutions). One must take special care to account for the different values of  $f_0$  which obtain in the different solutions by measuring these offsets with bare crystals. Even then, subtle changes in the boundary conditions can render such measurements suspect. For example, the exact position of the slip plane, which defines the position in the solution which moves with the same amplitude and phase as the underlying crystal surface, may not remain constant upon transfer from one solution to another. Also, the degree to which solvent trapping in pores at the surface occurs may change for a bare crystal and a coated crystal, so that simple subtraction of the offset may not always be possible. Other possible sources of discrepancy also exist. On the other hand, it has been amply demonstrated that when experiments involve only relative frequency changes which are measured in a given solution, the offset caused by the viscous loading has negligible effect on the accuracy of equation 8 for the determination of small mass changes.

### 3. Temperature dependence of oscillation

The intrinsic dependence of the resonant frequency of a quartz crystal on temperature

(T) is caused by changes in  $\rho_q$  and  $\mu_q$  with T. These effects are well known, and generally quite small, being around 1 Hz per °C depending on the particular cut of the crystal (2). In fact, the AT-cut is so popular partially because it is cut specifically to give a near zero T coefficient at room temperature. Thus, the intrinsic T dependence of the crystals is practically negligible in EQCM applications. However, much larger changes in  $f_0$  with T occur when crystals are immersed in solution due to the coupling of the acoustic shear wave into the solution as described above. Equation 18 shows that  $f_0$  is proportional to  $(\rho_l \eta_l)^{1/2}$  and allows calculation of the effect of changes in T given the density and viscosity as functions of T. For example, the values of  $\rho_l$  at 20 and 25 °C are 0.99823 and 0.99707 g cm<sup>-3</sup>, respectively, and the values of  $\eta_l$  at 20 and 25 °C are  $1.002 \times 10^{-2}$  and  $0.8904 \times 10^{-2}$  g cm<sup>-1</sup> s<sup>-1</sup>, respectively. Use of these values in equation 18 to calculate the expected change in  $f_0$  gives 41 Hz. This frequency change is larger than those for monolayer adsorption/desorption processes and not negligible with respect to those for solvent or ionic transport in thin films. Thus, in experiments in which the frequency is to be monitored at length, the temperature must be controlled to at least 0.1 °C, preferably to better than 0.02 °C. This is possible with commercially available temperature control baths and jacketed cells. On the other hand, measurement of short term, relative frequency changes (which might occur during a cyclic voltammetric experiment, for example) generally do not require such careful control of the temperature because the drift in T which can occur during a scan lasting only a few seconds is negligibly small.

#### 4. Viscoelastic deposits

An attractive use of the EQCM is to study the mass transport processes which occur during redox events in thin polymer films. Due to their large molecular weights and the resulting chain entanglement, to crosslinking (whether chemical or physical), and to solvent-induced swelling, these systems frequently exhibit viscoelastic behavior. It is extremely important to determine whether the viscoelastic nature of the deposit is

influencing the resonant frequency of the crystal oscillator, because the linear mass-frequency correlation discussed above will, in general, not hold under such conditions.

An excellent source for general information on the viscoelastic properties of organic polymers is the classic book by Ferry (43). In general, the viscosity and shear moduli of polymeric solids, gels, and solutions are functions of the frequency at which they are measured (43). The shear modulus ( $\mu$ ), a measure of the stiffness of the material, increases with frequency, while the viscosity ( $\eta$ ) tends to decrease with frequency. At MHz frequencies, polymeric systems will tend to have values for  $\mu$  which are lower than that for quartz due to their lower stiffness, while having values for  $\eta$  which are higher than that for quartz due to the possibility for viscous loss from translational motion of the chains relative to one another. Since rigid layer behavior will tend to prevail when  $\mu$  is large and  $\eta$  is small, the higher the frequency, the greater the chance of observing rigid layer behavior (i.e. the behavior of elastic, as opposed to viscous, deposits). Also, since  $\mu$  increases and  $\eta$  decreases below the glass transition temperature ( $T_g$ ), a knowledge of the  $T_g$  for the film material will be useful in gauging whether or not viscoelasticity in the deposit is influencing the resonant frequency of the EQCM. Films with  $T_g$ 's far above the temperature of the experiment will tend to behave more rigidly than those with lower  $T_g$ 's. Also,  $\eta$  will tend to increase for films when they are swollen by solvent. Thus, the conditions under which the measurements are made (high frequency, above or below  $T_g$ , swelling solvent or not, etc.) influence the degree to which rigid layer behavior prevails, and therefore, the extent to which mass changes can be inferred directly from  $\Delta f$  using the Sauerbrey equation or the Z-match method.

The quantitative connection between the material properties of the film (i.e.  $\mu$  and  $\eta$ ) and the behavior of the EQCM resonator has yet to be established for the important case of a thin film on the EQCM in a semi-infinite liquid, the configuration of most polymer

modified electrodes or thin film sensors based on the QCM. The problem is complex because the shear wave exists simultaneously in the quartz crystal, the thin film, and the adjacent solution, so reflection of the shear wave at several interfaces must be taken into account. It would be most worthwhile to solve this problem, because then  $\mu$  and  $\eta$  for the film could be calculated from the information provided by an impedance analysis of the film. This would allow for correlation of the electrochemical behavior of the film (i.e. charge transport rates, permeability, etc.) with the material properties of the film, clearly a worthy goal. Reed, Kanazawa, and Kaufman have recently solved the problem of a viscoelastic film of arbitrary thickness atop the QCM resonator, taking the piezoelectricity of the quartz explicitly into account (44). This contribution will be a valuable one, and will hopefully lead the way for an analysis which takes into account the shear wave propagation into the liquid adjacent to the film.

As was pointed out earlier, it is essential to determine whether or not the viscoelastic properties of the film influence the measurement. For example, if mass measurements are being made of a film deposition process, it is possible that as film thickness increases, the mass sensitivity may change due to excessive viscosity of the deposit (e.g. this would be a problem common to highly solvent swollen polymer films). There are several ways of checking for such effects.

One method is to verify that changes in deposit thickness or surface coverage scale linearly with changes in  $\Delta f$ . This requires that some parameter can be found which provides an independent measure of thickness or coverage, such as electrochemical charge, optical absorbance, ellipsometric functions, etc. Then, to the extent that the changes in these quantities scale with changes in the observed  $\Delta f$ 's, a good argument can be made that the measured  $\Delta f$ 's are a true representation of the mass changes occurring at the surface. However, many effects could obscure such comparisons, an example of which would be varying porosity or density of the deposit as a function of thickness (an effect

which is rather common in electrodeposited oxide and conducting polymer films).

A more straightforward and less ambiguous method relies on the dependence of the crystal Q on the viscosity of the deposit. Thus, measurements of Q during a film deposition will reveal the extent of changes in the deposit viscosity which can signal the potential for deviations from rigid layer behavior. In particular, as Q decreases due to increasing deposit viscosity, the width of the G versus f plot will increase above the value which arises from immersion of the bare crystal in solution. It is not yet clear how large this increase must be to generate significant deviation from equations 8 or 9, but the presence of detectable increases in Q (e.g. > 10%) should certainly give rise to the suspicion that such deviations might exist.

##### 5. Deposit roughness and porosity.

As mentioned above in the context of crystal surface finishes, roughness can cause large apparent mass loadings due to the liquid which is trapped within pores at the crystal surface. This can occur not only from roughness of the quartz crystal surface, but also from roughness which might exist in the deposit. Schumacher et al. (22) showed that such roughness in gold oxide deposits can cause very large discrepancies between the expected  $\Delta f$  and the observed value. They attempted to fit the discrepancies by modeling the surface as having hemispherical undulations which trapped solution, and further assuming that this trapped solution behaved as a mass rigidly attached to the surface (22). Although some disagreement between this model and the experimental data was observed, the general trends suggest that the qualitative features of the model are sound. In a later contribution, Schumacher et al. (23) gave other experimental examples of the appearance of such roughness effects for Ag and Cu surfaces following oxidation. They also showed that, for the case of Ag, prolonged application of sufficiently negative potentials caused the surface to become relatively smooth again, as judged by both the increase in EQCM frequency due to the loss of trapped solution and by differential capacitance measurements. Again,

however, quantitative predictions of the expected frequency changes from the roughness based on SEM observation of the roughened surfaces were not in agreement with the experimentally observed  $\Delta f$ 's.

Experiments recently done in these laboratories have also indicated that deposit morphology can influence the EQCM frequency response. The deposition and dissolution mechanisms of electrochromic films of diheptyliologen bromide (DHVBr) were studied using the EQCM (45). In this work, the dissolution at fast scan rates of the DHVBr films was shown to proceed by a pitting mechanism, with the pits eventually growing together over time so that the film disintegrated only late in the scan. This situation is shown schematically in Figure 8. To the extent that the solvent trapped within the pores has a density similar to that of the film, the frequency should only increase late in the scan, when the disintegration occurs. This is because the mass lost by film dissolution is replaced by the solution trapped within the pores. The observation of this behavior in the EQCM experiments prompted the proffering of a model for dissolution involving pit nucleation and allowed for a (rather speculative) assignment of pit nucleation as being progressive rather than instantaneous, based on the scan rate dependence of the frequency changes. This study serves as an example of the use of indirect EQCM information regarding surface roughness to help elucidate mechanistic details about the behavior of thin films.

In the measurement of monolayer mass changes, the magnitude of the observed frequency change is frequently so small that meaningful mass changes cannot be made using the usual experimental conditions. One way around this is to purposefully roughen the surface to increase the surface area of the electrode. Since the sensitivity to mass changes increases with the true surface area, this strategy makes it possible to increase the detection limit for mass changes linearly with the increase in surface area. Preliminary experiments have indicated the feasibility of this approach for sensitivity enhancements of

approximately a factor of two. Larger increases should be possible. A disadvantage of such an approach is that the measurement of absolute frequency changes cannot be made due to the relatively unpredictable effects of solvent trapping within the pores on the roughened surface.

Another possible source of frequency changes for thick films is porosity of the deposit. If a film is porous, then significant amounts of mass may be trapped within the pores of the film (i.e. in the void volume of the film). In this case the frequency decrease for deposition of the film will result not only from the mass of the film itself, but also from the mass of solution trapped within the pores. In the limit of microscopic pores, this model reduces to one of film swelling by the solvent or solution, so that all of the effects discussed above regarding film swelling hold here. To the extent that the film behaves elastically both with and without the trapped solvent, it is possible to calculate the amount of trapped solvent (and, therefore, the pore volume). This is done from the difference in the oscillation frequency of the crystal coated with the (dry) film in air and with the hydrated crystal in solution. For this calculation, the offset due to solution viscous loading must be corrected for, and, therefore, must be the same for the bare and coated crystal. For highly porous films, roughness effects will be important, so that these types of calculations will only be feasible for very thick films for which the contribution from surface effects (e.g. roughness) will be small in comparison to the total frequency change.

#### D. Correlations between frequency changes and electrochemical parameters

In correlating EQCM frequency changes with electrochemical data, it is useful to use different methods of data presentation. For convenience, the case of application of the EQCM to the study of a simple deposition process will be considered. An example would be the electrodeposition of Ag. The two important electrochemical parameters to compare to  $\Delta f$  are the charge ( $Q$ ) and the current ( $i$ ). The charge is an integral measure of the total number of electrons delivered at the interface during the process (reduction, in this case).

To the extent that each electron which is supplied results in the deposition of one atom of Ag, there should be direct proportionality between  $Q$  and  $\Delta f$ . This is shown by equation 19:

$$\Delta f = (10^6 \text{ MW } C_f Q) / (n F) \quad (19)$$

where  $n$  is the number of electrons transferred to induce deposition,  $F$  is the Faraday constant,  $MW$  is the apparent molar mass of the depositing species,  $C_f$  is the sensitivity factor for the crystal employed (see equation 8), and the factor of  $10^6$  provides for the unit conversion from  $\mu\text{g}$  in  $C_f$  to  $\text{g}$  in  $MW$ . A plot of  $\Delta f$  versus  $Q$  will give the apparent mass per electron of the deposited species, when  $n$  is taken into account. The corresponding equation for the relationship between  $i$  and  $\Delta f$  is:

$$i = \{d(\Delta f)/dE\} (10^{-6} n v F) / (MW C_f) \quad (20)$$

in which  $d(\Delta f)/dE$  is the derivative of  $\Delta f$  with respect to potential (for a cyclic voltammetric experiment),  $v$  is the scan rate, the factor of  $10^{-6}$  provides for unit conversion described above, and the other parameters have been described above. Equation 19 is useful for comparing total changes in oscillation frequency with electrochemical charges, while equation 20 is especially useful for the detection of subtle relationships between  $\Delta f$  and  $i$ . These equations will be used in the sections below to provide for detailed comparison between frequency and electrochemical parameters for various systems. Of course, electrochemical experiments other than cyclic voltammetry may be used in conjunction with the EQCM. The appropriate equations for these may be easily derived keeping in mind the proportionality between  $Q$  and  $\Delta f$ .

### III. Monolayer systems

#### A. Introduction

EQCM studies of the electrosorption of monolayer systems are an extremely challenging application of the technique due to the very small mass changes which occur. In addition to the electrosorption event, several other processes may contribute to the

observation of frequency changes, such as adsorption/desorption of solvent or supporting electrolyte ions during the electrosorption, changes in the position of the slip plane (i.e. the plane which defines the first layer of the adjacent medium which is not rigidly attached to the electrode surface) due to the electrosorption, and changes in the viscosity and/or density of the double layer induced by changes in composition as a function of applied potential. These effects have not yet been unambiguously observed, but few systems have been quantitatively studied as of yet.

One feature of monolayer systems which makes them somewhat more tractable is that, since the adsorbate layer is so thin compared to the wavelength of the shear wave in the resonator, the added mass from the electrosorbed layer should exist entirely at the antinode of the shear wave. Therefore, the adsorbate layer should experience no significant shear deformation, and its viscoelastic properties should have no influence on the measurement.

The studies which are described in this section demonstrate the detection of submonolayer mass changes during Faradaic processes at electrode surfaces. In most, mass changes are directly correlated with charge to gain insight into the compositional changes accompanying the interfacial charge transfer event. For example, it is possible to determine the electrosorption valency from such measurements. In other cases, deviations in the predicted correlations are speculatively attributed to the influence of solvent and/or ion association with the monolayer. Much remains to be done to elucidate how interfacial interactions contribute to the observed frequency change.

#### B. Electrosorption of oxides and halides on Au

The first application of the EQCM to the *in situ* measurement of mass changes from monolayer deposition or dissolution processes was by Bruckenstein and Shay (46) who studied the formation of the adsorbed oxygen monolayer at Au electrodes. They were able to observe frequency changes for this process as small as ca. 15 Hz with a signal to noise

of better than 50. A 10 MHz crystal operating in its fundamental mode was used in this study, for which the mass sensitivity is ca.  $1 \times 10^{-9}$  g Hz<sup>-1</sup>. Frequency decreases were observed for formation of the adsorbed monolayer, and these frequency changes were reversible in the sense that the original frequency was reattained when the adsorbed layer was removed by reduction. The agreement between the mass change predicted from the charge measurements and that inferred from the frequency change was better than 10%. Hysteresis between the time of passage of electrochemical charge and the observed mass change (i.e. 40% of the charge for a monolayer was passed before any mass change occurred) was used to support a postulated place exchange mechanism for O electrosorption which was consistent with a number of previously proposed mechanisms. This first application of the EQCM to the study of a monolayer system revealed the power of the technique for making detailed mechanistic proposals based on precise mass measurements during redox events at electrodes.

These workers also observed gradual frequency changes which occurred in the double layer region of the voltammetric scans. These frequency changes were speculatively attributed to changes in the structure of the double layer (e.g. adsorption of supporting electrolyte anions at potentials positive of the point of zero charge).

Schumacher et al. (22) also used the EQCM to study the formation of electrosorbed oxide layers on Au electrodes. These workers observed mass gain coincident with formation of the oxide layer, however, their conditions promoted the roughening of the surface, in contrast to those of Bruckenstein and Shay (46). As discussed in section II(5) above, this roughening caused larger than expected frequency decreases for oxide formation, especially in basic and neutral media. This result was confirmed in a later study by Stockel and Schumacher (27), who also observed that frequency decreases in aqueous sulfuric acid are smaller than expected. They postulated that place exchange only occurs in neutral and basic media, with monolayer discharge in acid perhaps accompanied only

by deprotonation of adsorbed water. While clearly of a speculative nature, these results point to the type of information available from the EQCM.

The electrosorption of bromide and iodide on Au electrodes was studied by Deakin et al. (47), who showed that full monolayer coverages were attained at sufficiently positive potentials. This conclusion followed from the evaluation of the mass changes which occurred during the electrosorption process and the geometric constraints imposed by the sizes of the halide ions. The slopes of plots of the charge for electrosorption versus surface coverage (obtained from the EQCM frequency change) were shown to provide the electrosorption valency,  $\gamma$ . Values for  $\gamma$  obtained in this way were reported as  $1.01 \pm 0.05$  for iodide and  $0.30 \pm 0.03$  for bromide, both in excellent agreement with previously reported values from other groups. This was one of the first reports to demonstrate the use of signal averaging methods for the acquisition of EQCM data, and clearly demonstrated the extension of the method to detailed, submonolayer mass/charge correlations.

### C. Underpotential deposition of metals

The first application of the QCM to UPD processes was by Bruckenstein and Swathirajan (48). These authors made ex situ measurements of mass changes due to UPD of Pb and Ag on Au electrodes by removing the QCM crystal from the cell following the deposition and measuring  $\Delta f$  for the dried crystal in air. They were able to determine the UPD coverage with quite good accuracy, as compared to parallel rotating disk and rotating ring disk electrode measurements. The reported accuracy was 5-10%. A 10 MHz crystal with a sensitivity factor of ca.  $0.227 \text{ Hz ng}^{-1} \text{ cm}^2$  was used in this study.

The first in situ application of the EQCM to UPD processes was the determination of the electrosorption valency for Pb UPD on Au by Melroy et al. (24). A value for  $\gamma$  of 2.0 was obtained by comparison of the total charge and the total mass gain for a scan over the UPD region. The accuracy for this determination was ca. 5%, and the value for  $\gamma$  was in good agreement with those previously reported. This study employed a 5 MHz crystal

driven at its third harmonic frequency (15 MHz) through the use of a tuned LC element in the feedback loop of the oscillator circuit, as described above (24). The use of the third harmonic provided a three-fold larger mass sensitivity than would have been obtained at the fundamental frequency, as shown by equation 8. In this case, the mass sensitivity was  $0.170 \text{ Hz ng}^{-1} \text{ cm}^2$ .

Deakin and Melroy (28) reported on a very detailed study of the UPD of Pb, Bi, Cu, and Cd on Au. They used a computerized apparatus which provided for facile manipulation of the frequency and electrochemical data. This allowed them to easily construct plots of charge versus mass, the slopes of which are equal to  $F\gamma/MW$ , providing a simple determination of  $\gamma$ . This analysis follows along the same lines as that used to arrive at equation 19. Further, they demonstrated the use of the derivative representation of  $\Delta f$  (see equation 20 above) for the direct comparison of the rate of mass change with the electrochemical current. The data in Figure 9 serve as an example of the type of information which can be obtained from such an analysis. The dashed line is the cyclic voltammetric current for a scan through the UPD region and into the region for bulk deposition of Bi. The solid line is generated from  $\Delta f$  using equation 20 and assuming that  $\gamma = 3$ . It is immediately evident that the voltammetric peaks which occur near 0.15 V are accompanied by mass changes which are much smaller than and in a direction opposite to expectations. The authors presented two possible explanations for this effect. Referencing to the negative scan, first, the current may be from further discharge of adsorbed (but only partially reduced) Bi, with a consequent desorption of weakly adsorbed anions. Second, the reduction may induce some change in electrode morphology which influences the coupling of the crystal to the solution, thereby changing the frequency in such a way as to obscure any mass flux which may accompany this reduction. A study of the anion dependence of this effect would be an obvious test of the first hypothesis, which seems the most reasonable of the two. At any rate, this study showed that use of the derivative

representation of  $\Delta f$  clearly allows one to observe very subtle relationships between current and mass flux.

#### D. Adsorption/desorption of surfactant molecules

Work in these laboratories has shown that mass changes associated with electrochemically induced changes in surface coverage of redox surfactants can be monitored using the EQCM (49,50). These redox surfactants are derivatives of (dimethylamino)methylferrocene ( $(CH_3)_2NCH_2Fc$  or DMAFc, where Fc is the ferrocene group) which have been quaternized at the amino nitrogen using 1-bromoalkanes having chain lengths ranging from 1 to 18 carbons. These are referred to by the number of carbons in the chain, so that the 18 carbon derivative would be called C18, the 12 carbon derivative, C12, and so on. This class of molecules was first reported by Saji et al. (51) who showed that these surfactant derivatives form micelles when the ferrocene group is present in its Fe(II) form (when the molecule is a cation), while oxidation to the Fe(III) form (the dication) results in disruption of the micelles. This behavior suggested that the tendency toward adsorption for these surfactants could also be electrochemically modulated, a notion which has since been verified (49,50).

Figure 10 shows results which are representative of this behavior. Curve A shows the cyclic voltammogram observed for a 22  $\mu M$  solution of C12. At this low concentration, the contribution to the current from diffusion is negligible, and the only response is from those molecules of C12 which are adsorbed at the Au electrode surface. Thus, a symmetric surface wave centered near 0.48 V is seen. Curve B shows the EQCM frequency response obtained simultaneously with the CV data. These data clearly show a loss of mass (frequency increase) coincident with the redox process at 0.48 V. Most of the mass is regained during the return scan, but over a slower time frame due to the slow delivery of C12 to the surface from this extremely dilute solution. For this same reason, the cathodic wave in the CV is smaller than the anodic wave.

The implication of these data is that the oxidation of C12 to its dicationic form results in its desorption, and a corresponding mass loss. Direct comparison of the mass loss with the charge required to electrolyze the adsorbed layer indicates that MW (see equation 19) is, within experimental error, equal to the molar mass of the surfactant derivative, excluding the mass of any counterion or solvent which may be associated with it. In other words, the frequency increase can be accounted for entirely from the electrochemically induced desorption of the surfactant itself.

The value of  $\Delta f$  of 3.2 Hz corresponds to a mass loss of  $53 \text{ ng cm}^{-2}$  or a loss of  $1.3 \times 10^{-10} \text{ mole cm}^{-2}$ . This is roughly half of a monolayer, based on a head group limited molecular area of 50 square angstroms (estimated using molecular models). It is clear from the signal to noise ratio in the figure that the detection limit is at least as small as 5% of a monolayer. These data were obtained with a 5 MHz crystal operated at its fundamental frequency, and are the average of 10 scans.

This very close agreement between predicted mass loss and charge consumed during desorption does not hold for other chain lengths. For example, for the C10 derivative, the mass loss is larger than predicted when the surfactant is present at submonolayer coverages (50). For the C14 derivative, the mass loss is also larger than predicted, but only after complete monolayer coverage has been achieved (These molecules exhibit Langmuirian adsorption isotherms with saturation at one monolayer (50).) These effects have been tentatively attributed to a) solvent incorporation into the monolayer for C10 at low coverages, so that the mass for desorption includes a contribution from loss of this trapped solvent and b) association of counterions with the high charge density C14 monolayer at saturation coverage so the mass for desorption includes a contribution from these tightly bound counterions. Such effects are not without precedent (50). While of a highly speculative nature, these proposals from preliminary studies of monlayer adsorption/desorption processes are indicative of the wealth of unique information which

is, in principle, available from the EQCM.

Another benefit of using the EQCM to study adsorption/desorption processes of such molecules is the ability to observe these processes in the presence of large excesses of solution phase species. Figure 11 illustrates this point (49). The voltammogram (curve A) shows clearly the wave for the C12 derivative in solution (0.5 mM). The surface wave for the adsorbed redox couple is not readily apparent due to the relatively large current for the solution phase couple. However, the EQCM frequency response shown in curve B clearly shows the mass loss which is a consequence of the oxidation of the surface species. Thus, the adsorption/desorption behavior of the adsorbed couple may be inferred from the mass flux, even under conditions in which the electrochemical response is dominated by the solution phase couple.

The longer chain derivatives (e.g. C16 and C18) are more strongly adsorbed at the Au electrode surface. Studies of the mass changes which occur during redox cycling of these tightly bound monolayers give more convincing evidence that ion association processes can be probed using the EQCM. Plate A of Figure 12 shows the voltammetry of a monolayer of adsorbed C16 at  $50 \text{ mV s}^{-1}$ . The morphology of the waves is similar to those described above and essentially invariant with scan rate. Plate B shows the corresponding EQCM data, but at three different scan rates. At the lowest scan rate, a smooth frequency increase like that in Figure 10 is observed, characteristic of mass loss during oxidation as described above. However, at higher scan rates, the frequency shows a pronounced decrease prior to this increase. This is attributed to a desorption rate for C16 which is slow enough on this time scale so that charge compensating anion insertion into the monolayer occurs prior to the ultimate desorption event (52). These rather speculative interpretations suggest that transient mass transport phenomena can also be observed with the EQCM, given the right conditions.

The objective of this section has been to demonstrate the various types of information

available from EQCM studies of monolayer systems, especially monolayers of redox molecules. Given that the application of the EQCM to monolayer assemblies is still in its infancy, and in light of the great current interest in such systems (see reference 50 and references therein) it seems clear that EQCM methods will make many important contributions to their understanding.

#### **IV. Multilayer deposition and dissolution**

##### **A. Introduction**

Studies of multilayer depositions and dissolutions have a long history in electrochemistry. Early interest focused on electrodeposition of metals. More recently, the deposition of semiconductor materials, the growth and cycling behavior of oxide layers, and the deposition and dissolution mechanisms of electrochromic films have been popular topics of investigation. While a great variety of phenomena is observed in the electrochemical responses of these diverse systems, many of these studies have probed processes common to all of them such as mechanisms of nucleation, growth, and dissolution, current efficiency for deposition and dissolution, the physical state of the deposit (i.e. roughness, porosity, etc.), and the stoichiometry of the deposit. In this section the use of the EQCM to provide this type of information for selected examples is described.

##### **B. Deposition and dissolution of electrochromic films of diheptylviologen bromide**

The highly colored deposits formed by reduction of various salts of N,N'-disubstituted-bipyridines have been widely investigated due to their potential applications in electrochromic devices. Recently, Ostrom and Buttry (45) used the EQCM to study the mechanisms of deposition and dissolution for films of 1,1'-diheptyl-4,4'-bipyridinium bromide (diheptylviologen bromide (DHVBr)) under both potential step and sweep conditions. As discussed in section II.5. above, under potential sweep conditions, the observed frequency changes during dissolution were consistent with

a pitting mechanism in which deposit roughness increased during dissolution followed by film disintegration late in the dissolution process. This conclusion was based on the observation of large apparent mass loading due to the trapping of supporting electrolyte within small pores in the film. As will now be discussed, deposition under potentiostatic conditions also causes large apparent mass loadings which can be attributed to nucleation processes.

When deposition under potentiostatic conditions occurs, the rate of growth of the deposit is controlled by the delivery of reactant to the surface and the nucleation rate, which is usually a function of the applied potential. Both the charge ( $Q$ ) consumed in the deposition and the value of  $\Delta f$  provide information about the deposition.  $Q$  reveals the cumulative amount of deposited material (assuming 100% current efficiency) while  $\Delta f$  gives a measure of the total mass loading from the deposit and from solvent or supporting electrolyte which might be associated with the deposit (i.e. trapped in pores or incorporated into the bulk of the deposit). Thus, comparison of  $Q$  and  $\Delta f$  can allow for evaluation of current efficiency, film composition, and film roughness, under the proper conditions.

For a diffusion controlled deposition under conditions of 100% current efficiency and a uniform, smooth deposit, the equation which describes the time dependence of  $\Delta f$  is:

$$\Delta f = (2 \times 10^6) C_f \text{MW} D^{1/2} C t^{1/2} \pi^{-1/2} \quad (21)$$

where  $D$  is the diffusion coefficient for the diffusing species (in  $\text{cm}^2 \text{s}^{-1}$ ),  $C$  is the concentration (in  $\text{mole cm}^{-3}$ ),  $t$  is time (in s), and the other quantities have been previously defined. This equation comes from the combination of equation 19 above and the integrated Cottrell equation. Note that MW is the apparent molar mass of the depositing species. It might include contributions from solution which is trapped or incorporated within the deposit or from deposit roughness. When linear plots of  $\Delta f$  versus  $t^{1/2}$  and  $Q$  versus  $t^{1/2}$  are obtained, it is possible to directly compare their slopes to get MW:

$$(S_f / S_q) (10^6 F / C_f) = MW \quad (22)$$

in which  $S_f$  is the slope of the  $\Delta f$  versus  $t^{1/2}$  plot (in  $\text{Hz s}^{-1/2}$ ),  $S_q$  is the slope of the  $Q$  versus  $t^{1/2}$  (in  $\text{C cm}^{-2} \text{ s}^{-1/2}$ ). Alternatively, plots of  $\Delta f$  versus  $Q$  provide MW directly, as described above. These methods have the advantage of not requiring knowledge of  $D$  or  $C$  for the determination of MW.

Figure 13 shows the results of a potential step experiment over the first reduction wave of DHV. Curve A is the plot of  $\Delta f$  versus  $t$  and Curve B is the plot of  $\Delta f$  versus  $t^{1/2}$ , the microgravimetric equivalent of an Anson plot. Curve B shows that  $\Delta f$  varies with  $t$  with essentially the same functional dependence as does  $Q$ , in accordance with equation 21. Table 1 shows the values for MW obtained for several potential step experiments of this type. Recalling that the peak potential is at ca. -0.55, the data in the table show that the value of MW depends very strongly on the final potential for the step. Steps far over the wave give values for MW which are quite close to the molar mass of DHVBr (434.5 g  $\text{mol}^{-1}$ ), while steps to the foot of the reduction wave give values as much as a factor of three larger than this. This behavior has been attributed to the number of nucleation sites for film growth formed during the reduction (45). For steps to very negative potentials well past the wave, the number of nuclei formed is large, so that film growth is relatively uniform. For steps to the foot of the wave, only a small number of nuclei are formed. These nuclei grow hemispherically with time, and, as a consequence of this, the effective surface roughness of the electrode is increased. As discussed above, this increase in surface roughness should result in large apparent mass loadings, and values of MW which are larger than the molar mass of the depositing species. This coupling of adjacent solution to the deposited nuclei is schematically depicted in Figure 14. (Note that the degree to which the solution is coupled to the surface is unknown, and should not be inferred from the figure, which serves only to illustrate the effect.) This model qualitatively predicts that the smaller the overpotential, the smaller the number of nuclei, and, therefore, the greater

the extent of coupling of the adjacent solution to the surface. This will lead to larger values of MW, in agreement with observations. Quantitative predictions are not possible at the present time, but the development of the theory for such a case would undoubtedly prove useful in the study of nucleation and growth processes for other systems.

The value of MW obtained for steps well past the wave (ca. 460 g mol<sup>-1</sup>) is quite near to the molar mass of DHVBr. This is strong evidence that at large overpotentials the film deposits relatively uniformly and with little incorporated solvent or supporting electrolyte. Such information on the solvent content and surface morphology of electrodeposited films is extremely difficult, if not impossible, to obtain using other techniques. However, these investigations have shown that the EQCM is uniquely well suited for such determinations.

### C. Other systems

Grzegorzewski and Heusler (53) recently published a study in which they used the EQCM to study the mass changes which occur during the redox cycling of MnO<sub>2</sub> films. A particularly novel aspect of this investigation was their construction of a rotating EQCM, thus allowing for the facile control of mass transport to the electrode surface. Through detailed correlations of mass and charge they were able to show that redox cycling of the oxide causes transfer of manganese ions and oxygen ions across the oxide/electrolyte interface in independent processes. They also showed that, in steady state, only electronic currents flow through the oxide, while in transient experiments ionic transport occurs with corresponding changes in the oxide stoichiometry. Using essentially the same analysis as that implied by equation 19, they were able to calculate the molar mass of the species associated with oxygen transfer across the oxide/electrolyte interface. A value of 144 g mol<sup>-1</sup> was obtained, suggesting that the oxygen ions were transferred with several molecules of water. As will be discussed below in the context of mass transport during redox events in thin polymer films, the observation of solvent transfer is not uncommon in thin films. However, it is important to note that such transfers should not be considered to

be measures of hydration numbers. Rather, these transfers are a consequence of varying thermodynamic activities of water and other components within the film during the redox events (54).

Reynolds, Rajeshwar and coworkers (55) have used the EQCM to study the deposition and dissolution processes which occur during the electrochemistry of  $\text{HTeO}_2^+$  at gold electrodes. The EQCM mass changes, when compared to the electrochemical charges, allowed identification of the direct  $4 \text{ e}^-$  reduction of  $\text{HTeO}_2^+$  to Te with the simultaneous deposition of the Te. Using the analysis suggested by equation 19, the  $n$  value for the reduction was found to be 3.6. This value was consistently lower than the value of 4 expected, which was attributed to a competing  $2 \text{ e}^-$  pathway (55). Further reduction of Te to  $\text{H}_2\text{Te}$  caused loss of mass due to the dissolution of the  $\text{H}_2\text{Te}$ . Both this study and the previous one on  $\text{MnO}_2$  amply demonstrate the dramatic enhancement of interpretive capability towards mechanistic assignments in deposition, dissolution, and redox switching of thin films provided by the availability of simultaneous, quantitative mass measurements.

## V. Polymer Films

### A. Introduction

Much of the work with the EQCM to date has been on the study of mass transport processes which accompany redox processes in polymer films on electrodes. Such systems have been recently reviewed (56), and only those aspects of their behavior pertinent to their study using the EQCM will be discussed here.

Much of the work on polymer modified electrodes (PME's) has focussed on the process of charge propagation through the polymer film. In the context of these studies, many suggestions have been made regarding the nature of the rate limiting processes for the charge propagation (56). Aside from the physical diffusion of the redox species through the film and the electron exchange reaction between redox groups, the transport of

solvent and/or supporting electrolyte through the films have been suggested as potentially rate limiting processes. Thus, a significant incentive for the study of ion and solvent transport through polymer films is to understand their role (if any) in the kinetics of charge propagation.

Ion and solvent transport may also play a role in determining the thermodynamic behavior of PME's in the sense that the conditions which produce non-unity activity coefficients for immobilized or incorporated redox groups may be somehow linked to these transport processes. Thus, the deviations from Nernstian behavior frequently observed for such systems (56) might be better understood given detailed information about compositional changes which occur during the redox reactions of the films.

In the next section, the mass transport processes which occur during redox reactions in polymer films containing redox groups are examined. Both organic and inorganic polymers are discussed. In the following section, the mass transport processes which occur during oxidation and reduction of conducting polymers are described. The emphasis in these sections is on a demonstration of the types of phenomena which can be observed for such systems using the EQCM. Examples of such phenomena include: current efficiency for deposition in electropolymerization reactions, extent of swelling of the film and changes in swelling which occur during redox reactions, ion transport, and changes in the viscoelastic properties of the deposit. Because changes in  $\Delta f$  can be measured relatively rapidly (ca. every 10 milliseconds) the kinetics of these processes will be accessible in some instances, although little has been done in this area to date.

### B. Redox polymers

#### 1. Poly(vinylferrocene)

The first report of use of the EQCM for measurement of mass transport processes in redox polymers films concerned the direct observation of ion and solvent transport in thin films of poly(vinylferrocene) (PVF) (57). Figure 15 (57) shows an example of the results

of such experiments. Curve A shows the CV obtained on a PVF film in 0.1 M  $\text{KPF}_6$ . Curve B shows  $\Delta f$  versus E for the scan. The EQCM frequency is seen to decrease substantially during the oxidation process, with reduction causing the frequency to reattain its original value. Comparison of the total  $\Delta f$  with the total charge consumed during the oxidation reveals that exactly one  $\text{PF}_6^-$  anion is inserted into the film for each electron removed. No evidence for solvent transport is observed, because the EQCM frequency change matches exactly that predicted for the insertion of the appropriate number of anions, based on the charge. Thus, charge compensation is achieved by the influx of anions which serve to neutralize the ferrocenium sites created during oxidation. This behavior is the simplest type which can be observed for such systems, i.e. unidirectional transport with no accompanying solvent. As discussed below, such behavior is more the exception than the rule.

Ward (32) described a study of the mass changes which occur during open circuit reactions of PVF with oxidants in solution. He found that the values for  $\Delta f$  which were observed for certain cases were much larger than expected, and attributed these to simultaneous solvent and anion transport. This represents a second class of behavior. Figure 16 shows an example of this (58). The experiment is similar to that in Figure 15, except that the solution contains 0.1 M  $\text{KIO}_3$ . The inner (smaller) curve is the CV and the outer curve is the derivative representation of  $\Delta f$  calculated assuming unidirectional transport of  $\text{IO}_3^-$  to maintain neutrality and no accompanying solvent transport (see equation 20). When viewed in this way, the extent to which the  $d(\Delta f)/dE$  curve is larger than the cyclic voltammetric current is an indication of mass changes which are in excess of those expected for simple anion ( $\text{IO}_3^-$ , in this case) insertion. Thus, it is clear that the EQCM frequency changes for this system are far in excess of those expected based on the amount of charge consumed during the oxidation, probably as a result of solvent transport in the same direction as the anion transport. However, such results are not unambiguous,

and additional information is required to arrive at a definitive description of the mass transport processes. Furthermore, impedance measurements made on this system in both the oxidized and reduced forms reveal a significant decrease in  $Q$  (by a factor of ca. 1.5) after oxidation in  $\text{KIO}_3$  electrolyte, indicative of the onset of viscoelastic behavior for the deposit (58). Thus, quantitative calculation of mass changes from  $\Delta f$  is suspect in this particular instance. Even with such uncertainty in the quantitative description of the transport processes, it is certainly reasonable to conclude from such data that anion and solvent transport occur simultaneously and in the same direction. This is especially true since the unambiguous observation of the onset of viscoelastic behavior following oxidation is almost certainly a consequence of solvent swelling (43).

A third class of behavior is exemplified by the data in Figure 17 (57). In this case, the oxidation of the film is carried out in a solution of 1.0 M  $\text{NaCl}$ . Very large increases in frequency (mass loss) are seen to accompany oxidation. These were attributed to the dissolution or delamination of the PVF film following its oxidation. It has since been discovered that very high molecular weight or crosslinked PVF does not leave the surface after oxidation. Rather, it behaves similarly to films oxidized in  $\text{IO}_3^-$  containing electrolyte, in which extensive solvent swelling occurs (58).

These experiments show that the behavior of these films follows simple trends which derive from the solubility properties of the monomeric ferrocenium cation in aqueous solution, in that more swelling seems to occur in supporting electrolytes in which the cation would be more soluble. The ability to directly observe such qualitative trends represents a significant step forward towards the goal of rational manipulation of the behavior of such deposits. These data also point out the importance of considering the possibility of simultaneous transport of different species (both solvent and ionic) during the redox reaction. As discussed earlier, there is no a priori reason why these transport processes should occur in any given direction. Rather, the directions in which the various

species will flow is entirely dependent on the changes in their thermodynamic activities which occur within the film as a result of the redox reaction, as recently pointed out by Bruckenstein and Hillman (54). Thus, the simple models of ion insertion and expulsion which derive from considerations of electroneutrality serve only as starting points for a more detailed analysis. Finally, these results reveal a need to more fully understand the factors which dictate the directionality and extent of the various transport processes which can occur in such systems.

## 2. Nickel ferrocyanide films

Thin films of nickel ferrocyanide have been studied for some time in regards to the remarkable sensitivity of the formal potential for the immobilized Fe(III)/Fe(II) redox couple to the identity of the cation of the supporting electrolyte (59). A recently published EQCM study of such films (60) has provided the first quantitative, unambiguous measurement of solvent transport in thin films on electrodes. Quantitative determination of the extent of solvent transport during the redox process for such films was achieved by measuring the difference in the total mass change (comprised of contributions from both ion and solvent transport) which results from use of isotopically substituted solvent.

As has been reported in an EQCM study by Feldman and Melroy (61), oxidation of the Fe(II) sites in Prussian Blue films (the iron analog of the nickel ferrocyanide system) results in expulsion of cations from the lattice (and vice versa) as judged by the observation of mass loss during oxidation in EQCM experiments on this system. Discrepancies between the mass loss predicted based on charge consumption and that observed were suggestive of solvent incorporation following cation expulsion. The good stability of the Prussian Blue films (61) and their analogs (59) and their demonstrated permselectivity towards cation transport (59) suggested the possibility of indirect determination of solvent transport using isotopically substituted solvents, since both film stability and permselectivity are essential to this particular experiment.

Figure 18 (60) shows the results of such an experiment. Curves a and b in the upper plate are the cyclic voltammograms for the nickel ferrocyanide film in 0.1 M CsCl/H<sub>2</sub>O solution and 0.1 M CsCl/D<sub>2</sub>O solution, respectively. The CV's were obtained sequentially by transfer from the H<sub>2</sub>O solution to the D<sub>2</sub>O solution. The CV's track each other exactly, indicating that equal numbers of Fe sites are electrochemically accessible in these two media. Curves a and b in the lower plate show the EQCM frequency changes observed during the redox reactions in the H<sub>2</sub>O and D<sub>2</sub>O solutions, respectively. That the frequency increases during the oxidation and decreases during the reduction is expected based on the cation transport model discussed above. However, the mass loss (frequency increase) predicted from the charge consumed in the CV's was considerably greater than that observed, suggesting the presence of some other mass transport process which occurs in the opposite direction. The different values of  $\Delta f$  observed in H<sub>2</sub>O and D<sub>2</sub>O confirm this conclusion.

Figure 19 shows a schematic representation of the frequency changes observed during the CV's shown in Figure 18. The electrochemical charge is used to predict the mass loss for the expulsion of Cs<sup>+</sup> ions during the oxidation process, assuming unidirectional transport (i.e. a permselective film with a transport number for Cs<sup>+</sup> of 1). The predicted value is 224 Hz. The observed values in H<sub>2</sub>O and D<sub>2</sub>O are 125 and 115 Hz, respectively. The discrepancies between the observed values and the predicted values are 99 and 109 Hz, respectively. If the entire discrepancy were due to solvent transport, then the discrepancy for the D<sub>2</sub>O case should be 10% larger than that for the H<sub>2</sub>O case, exactly as is observed. Thus, the expulsion of Cs<sup>+</sup> cations is accompanied by the incorporation of significant amounts of solvent. The observed frequency changes are quantitatively predictable based on a model involving cation and solvent transport, verifying the permselectivity of these films (i.e. the absence of anion transport). It is especially significant that such detailed, quantitative determinations of solvent transport can be made

in the presence of simultaneous ion transport.

### C. Conducting polymers

#### 1. Introduction

A great deal of study has been done on the redox reactions responsible for the insulator to conductor transitions of conducting polymers. In particular, the rate of the switching process has, in some instances, been correlated with the identity of the ionic species in the supporting electrolyte (62,63). Thus, the identification of the species undergoing transport during the switching reaction is of considerable importance to the ultimate goal of manipulating the properties of these interesting materials for the many applications in which their use is envisioned. The EQCM is an excellent tool for such studies, and has been used in a number of cases already. Additional information which is available from EQCM measurements is the current efficiency for the electropolymerization process which is sometimes used to produce thin films of conducting polymers. This is especially useful since, up until recently, the charge consumed in the electropolymerization was used for the indirect determination of the amount of deposited material. This procedure will only be appropriate if the current efficiency is constant when different conditions are used (e.g. supporting electrolyte, solvent, or applied potential or current), a situation which will not be true in general. In contrast, the EQCM provides a direct measure of the mass of deposited material. Also, as will be described below, certain mechanistic questions regarding the electropolymerization can be more easily addressed given direct information on the amount of deposited material produced under different conditions. Finally, the EQCM can provide a qualitative, and sometimes quantitative, picture of the extent of solvent swelling or deswelling which occurs during the switching process for these films. Such data can be very useful in determining the energy density of conducting polymers in relation to their use in charge storage applications.

## 2. Poly(pyrrole)

The first reported study of ion transport during the switching reaction of a conducting polymer was on poly(pyrrole) (64). Oxidation of the insulating (neutral) poly(pyrrole) film to its conducting (cationic) state was shown to be accompanied by anion insertion, and reduction by anion expulsion. An exception was found for the case of tetrahydrofuran solvent with lithium perchlorate supporting electrolyte. In this instance, the first oxidation following electropolymerization was accompanied by anion insertion, but subsequent switching was accompanied by  $\text{Li}^+$  transport with the  $\text{ClO}_4^-$  remaining trapped within the film. The lack of  $\text{ClO}_4^-$  transport was attributed to strong interactions of this ion with the charged sites on the poly(pyrrole) backbone when in its conductive (oxidized) state. This demonstrated the importance of the solvent in mediating the electrostatic interactions of the counterions with the charged sites on the polymer chains, because the effect was only observed for  $\text{LiClO}_4$  in THF, not in acetonitrile.

A detailed method for determining current efficiencies for electropolymerizations was described by Baker and Reynolds (29) who applied this to a study of the deposition of poly(pyrrole). Measurement of changes in current efficiency as a function of the reactant concentration was shown to give information valuable in the interpretation of the mechanism of the electropolymerization. They gave a modified version of Faraday's law:

$$Q = n F m / MW \quad (23)$$

where  $Q$  is the charge consumed in the electropolymerization process,  $n$  represents the number of moles of electrons required to deposit one mole of monomer units,  $m$  is the cumulative mass change for the deposition, and  $MW$  is the apparent molar mass of the deposited species. The value of  $n$  can be viewed as a measure of the current efficiency for the deposition. It is important to note that the value of  $MW$  contains the mass of deposited pyrrole units, the mass of any dopant anions which are contained in the film by virtue of its partial oxidation to the conductive state at the electropolymerization potential, and the

mass of any solvent contained in the film. The degree of oxidation can be obtained by elemental analysis of a bulk sample of the film (29), but the amount of solvent incorporation is more difficult to obtain. In the absence of such information, a value of zero was used. Then, the value of  $n$  is obtained from  $Q$ ,  $m$ , and the assumed value of MW. This value of  $n$  is an upper limit due to the possible contribution of solvent to the observed mass change. Since the value of  $n$  is inversely proportional to the current efficiency, this procedure provides a lower limit on the current efficiency.

For a typical electropolymerization, plots of  $Q$  versus  $m$  were linear, with a slope proportional to  $n$  (29). It was found that  $n$  varied with the solution concentration of pyrrole from 5 electrons per pyrrole unit at 10 mM to 2.3 electrons per pyrrole unit at 100 mM. Measurements over a wide range of concentration showed that the electropolymerization rate depends on the square of the pyrrole concentration, in agreement with a proposed mechanism for electropolymerization which involves a second order coupling reaction between two pyrrole radical cations (29). This set of experiments represents a particularly elegant example of the power of the EQCM for mechanistic studies of processes which induce mass changes through deposition or dissolution processes at the electrode surface.

### 3. Poly(aniline)

The EQCM has been used to study the electropolymerization and transport processes during switching for thin films of poly(aniline) (26). Figure 20 shows an example of such an experiment. Curve A is a CV obtained for a scan recorded in the middle of an electropolymerization. The sharp anodic wave at ca. 0.15 V is the characteristic signature of the insulator to conductor transition for this and other conducting polymers. The broad cathodic wave at ca. 0.05 V is from switching back to the insulating state. These responses arise from the poly(aniline) which is already present on the electrode surface. The current passed above 0.6 V is from oxidation of anilinium monomer in solution, which ultimately results in the deposition of additional poly(aniline). Curve B shows  $\Delta f$  versus  $E$  for the

scan in Curve A. The decrease in frequency seen to begin at the onset of the anodic switching process and continue until the scan reversal indicates mass gain during the switching and charging processes (26). As seen by the frequency increase (mass loss) during the return scan, the mass gain from these processes is reversible. Additional mass gain occurs immediately after the scan reversal (between 0.7 and 0.55 V) which is the result of the deposition of additional poly(aniline) as a consequence of the oxidation of anilinium monomer between 0.6 and 0.7 V. The frequency at the end of the scan is lower than its initial value by 10 Hz due to this deposition. This amount of mass gain corresponds to roughly 1.0 nm of new film growth during the scan. The changes in frequency which occur during repetitive scans can also be used to monitor the course of the deposition (26).

Considerable detail regarding the electropolymerization process can be obtained from such measurements. For example, by measuring the total charge consumed during the deposition and comparing this with the total mass change, it is possible to obtain a measure of the current efficiency for the deposition. This was done for deposition of poly(aniline) at constant potential and by potential cycling, and current efficiencies of 15% and 40%, respectively, were calculated assuming a one electron oxidation of the anilinium monomer for the electropolymerization process (26). Such measurements provide a relatively simple way to optimize the deposition conditions for maximum current efficiency.

#### 4. Copolymers and composite polymer films

As mentioned earlier, a goal of the study of ion and solvent transport during the switching reaction for conducting polymers (and, in fact, for all thin films which undergo useful redox reactions) is that the information provided from such studies might be used for the rational manipulation of their properties to enhance the switching rates, improve the energy density, or in other ways induce the materials to have more desirable

characteristics. Two recent studies serve as examples of the use of the EQCM to aid in the correlation of ion transport with overall charge transport rates. These studies show that, given such information, the rational manipulation of charge transport rates is, indeed, possible.

In the first example, Reynolds and coworkers (63) electrochemically synthesized copolymers of pyrrole and 3-(pyrrol-1-yl)propanesulfonate in which the pendent sulfonate groups are neutralized with either  $\text{Li}^+$ ,  $\text{K}^+$ , or possibly  $\text{H}^+$ . Use of the EQCM to monitor ion transport during the switching process for such films demonstrated conclusively that cation transport was the dominant ion transport process during the switching reaction. Thus, the generation of anionic sites for the compensation of the cationic charges along the polymeric chains created by the anodic doping process is the result of expulsion of the anions which had originally been associated with the pendent sulfonate groups. Having definitively demonstrated a system in which unidirectional ion transport occurs, the dependence of overall charge transport rates on the identity of the cationic component of the supporting electrolyte was investigated. Faster charge transport was observed for  $\text{Li}^+$  containing electrolytes than for tetrabutylammonium ( $\text{TBA}^+$ ) containing electrolytes. That the faster rates occur for the cation with the smaller solvated radius ( $\text{Li}^+$ ) is consistent with a model in which the cation mobility is somehow involved in determining the overall charge transport rate. In this particular system, the sulfonated copolymer exhibited slower overall charge transport rates than did poly(pyrrole). However, the study did demonstrate the feasibility of controlling the identity of the ionic species undergoing migration during the switching reaction.

A second example of the application of the EQCM to help elucidate the directionality of ion transport and the use of such information to manipulate charge transport rates was a study of composite films of Nafion and poly(aniline) (65). Earlier work on ion transport during switching in poly(aniline) revealed that anion transport was dominant at pH's

above 0 (26). It was thought that higher charge transport rates could be attained by manipulating the ion transport in such a way as to achieve electroneutrality via proton transport. The reasoning behind this notion was that the higher mobility of the proton compared to other ions would allow for faster switching. Towards this end, poly(aniline) was electropolymerized within precast films of Nafion, a perfluorosulfonated polymer with good permselectivity for cation exchange. To the extent that this permselectivity precludes the rapid transport of anions within the Nafion film, the switching reaction should be accompanied solely by cation transport. As in the previous study, these cations would be in the film as the counter ions of the fixed sulfonate sites of the Nafion matrix. In acidic solutions, protons would be the only available cations, so they should be the only species undergoing transport. This situation is shown schematically in Figure 21.

Such a model of ion transport based on the maintenance of electroneutrality is obviously a highly simplified view of the possible mass transport processes which can occur in such films during redox switching. This is especially true in light of the recent work by Bruckenstein and Hillman (54), who presented a thermodynamic analysis demonstrating that electroneutrality alone cannot account for all of the transport processes in thin films. They show that, at equilibrium, the net ion and mass transport processes which result from switching are dictated by the activities of the various species. The implication of this work is that, for the general case, net transport can occur in either direction and that the relative molar proportions of the transporting species need not be integer numbers with respect to the number of moles of electrons transferred into or out of the film. However, under transient conditions it is possible that kinetic limitations can be created by the need to achieve electroneutrality (66), so that manipulation of rates should be possible for some systems by controlling the identities of those species which can fulfill this need.

Contrary to the previous results on simple (non-composite) poly(aniline) films (26),

and in agreement with expectations for the composite films, the switching process in these composite films showed no detectable evidence of anion transport. Figure 22 shows a CV/EQCM experiment for a Nafion film in which poly(aniline) has been grown to a thickness of roughly half of the Nafion film thickness. In this case, all of the poly(aniline) is contained within the interior of the Nafion matrix. As can be seen, scanning through the potential region of the insulator to conductor transition causes no detectable frequency change. This fact was attributed to the predominance of proton transport. Thus, to the extent that electroneutrality in this permselective system is achieved by proton transport with little accompanying solvent transport (an unproven, but not unreasonable, supposition) the observed mass changes should be extremely small due to the small mass of the proton. Another possible explanation derives from the possibility of fortuitous compensation of mass changes which occur in opposite directions. For example, if the Nafion film were not fully permselective, then a net mass change of zero could arise from simultaneous anion insertion and cation expulsion. Such an explanation is not without merit, but the favored model is that of proton transport, since the permselectivity of Nafion films is well known and widely exploited.

An additional explanation for the lack of detectable mass changes during switching in this system would be the loss of mass sensitivity due to shear wave attenuation within the Nafion matrix (65). If the shear wave were significantly damped within the region of the film close to the electrode surface, mass sensitivity would be lost in regions of the film well past the propagation length of the shear wave. This would occur because only that region of the film which experiences acceleration parallel to the electrode surface can contribute to the EQCM frequency response. This influence of penetration depth of the shear wave into the film has been previously observed in a QCM study of curing in photoresist films (67). In order to exclude this possibility in the present system, the mass changes in composites in which the poly(aniline) had been grown to thicknesses well

beyond the Nafion/solution interface were examined. For such films, that fraction of the poly(aniline) which extends into the solution, past the boundary of the Nafion film), exhibits "normal" mass changes which are characteristic of anion insertion/expulsion in the previously studied (non-composite) poly(aniline) films. This observation rules out the possibility of significant shear wave attenuation within the Nafion matrix, because in such a situation there could be no EQCM frequency response from mass changes in regions of the film much past the attenuation length. Thus, proton transport still seems the most likely explanation for the observed effects.

In order to more definitively demonstrate the presence of cation transport in these composite films, the mass changes in  $\text{Cs}^+$  containing supporting electrolyte solutions were measured. As shown in Figure 23, these data provide additional evidence for cation transport. ( $\text{Cs}^+$  containing electrolyte was used in this experiment to generate the maximum possible mass change from the cation transport process.) Mass loss was observed during the oxidation of the poly(aniline)/Nafion composite (and vice versa) consistent with  $\text{Cs}^+$  expulsion. The mass changes observed for the switching process in this medium were not as large as expected based solely on cation expulsion to maintain electroneutrality. Instead, smaller changes were observed, indicative of mixed cation and anion transport and/or cesium and proton transport (the experiments were conducted at pH 3 so the poly(aniline) would not be too resistive (26,65)) and/or concurrent solvent transport. Thus, considerable ambiguity remains as to the quantitative details of the mass transport process(es) for this system. Nevertheless, the data are reasonably convincing of the presence of a considerable component of cation transport for these composite films.

Based on the supposed predominance of proton transport for these composite films, their charge transport rates were compared to those of the simple (non-composite) poly(aniline) films using potential step experiments. The influence of pH was also examined to test for dependence on the relative proton concentration within the composite

film. Depending on the pH, these composite films exhibited charge transport rates as much as a factor of two larger than those of the simple (noncomposite) poly(aniline) films. The enhancement has been attributed to the predominance of proton transport in the composite films (65). Thus, this study represents an excellent example of how the understanding of charge transport mechanisms can be used in the rational manipulation of these processes.

## VI. Future Applications of the EQCM

This review has attempted to provide an entry into the application of the EQCM to problems of interest to the electrochemical community. As can easily be seen, many types of phenomena can be studied, some of which are not amenable to observation by other methods. In this respect, the EQCM represents a powerful new addition to the electrochemist's repertoire of characterization methods. However, the information obtained from the EQCM measurement is limited in that quantitative information is still only available on mass changes at the surface, and then, only when certain criteria are met. It seems likely that as additional theoretical treatments become available, it will be possible to extract some material properties of surface films using the impedance analysis methods described above. In this way, it might be possible to correlate some electrochemical or transport parameters (e.g. permeation, charge transport rates, etc.) with the microscopic relaxation processes upon which these material properties depend.

Despite the relatively non-specific nature of the information provided by the EQCM, its low cost and simplicity make it quite attractive for the determination of compositional changes at the electrode surface. An additional, significant attribute which it possesses is the high precision of the measurement of changes in frequency and impedance parameters. The method will prove especially useful when used in conjunction with other methods for interface characterization, such as surface enhanced Raman spectroscopy, infrared spectroscopy, ellipsometry, etc. In such multi-technique studies, the availability of a tool for such precise mass measurements will undoubtedly be of value, especially when the

quantitative aspects of the spectroscopic probes are in question.

**Acknowledgements** - We are grateful to the Office of Naval Research for the generous support of our efforts in the application of the QCM to electrochemical problems. Also, many thanks are due the coworkers whose hard work made this contribution possible.

## References

1. G. Sauerbrey, Z. Phys., 155:206 (1959).
2. Applications of Piezoelectric Quartz Crystal Microbalances (C. Lu and A. W. Czanderma, eds.), Methods and Phenomena Vol. 7, Elsevier Science Publishing, New York (1984).
3. P. L. Konash and G. J. Bastiaans, Anal. Chem., 52:1929 (1980).
4. T. Nomura, Anal. Chim. Acta, 124:81 (1981).
5. J. L. Jones and J. P. Meiure, Anal. Chem., 41:484 (1969).
6. J. P. Meiure and J. L. Jones, Talanta, 16:149 (1969).
7. T. Nomura, T. Nagamune, K. Izutsu, and T. S. West, Bunseki Kagaku, 30:494 (1981).
8. T. Nomura and M. Iijima, Anal. Chim. Acta, 131:97 (1981).
9. D. Salt, Hy-Q Handbook of Quartz Crystal Devices, Van-Nostrand Reinhold, Berkshire, England (1987).
10. R. D. Mindlin, Q. Appl. Math., 19:51 (1961).
11. H. J. McSkimin, P. Andreatch, and R. N. Thurston, J. Appl. Phys., 36:1624 (1965).
12. S. Bruckenstein and M. Shay, Electrochim. Acta, 30:1295 (1985).
13. H. K. Pulker and W. Schadler, Nuovo Cimento, 57B:19 (1968).
14. H. K. Pulker, E. Benes, D. Hammer, and E. Sollner, Thin Solid Films, 32:27 (1976).
15. H. Bahadur and R. Parshad, Physical Acoustics (W. P. Mason and R. N. Thurston, eds.), Academic Press, New York, Vol. 16, pp. 37-171 (1982).
16. G. Sauerbrey, Proc. Annu. Freq. Control Symp., 21:63 (1967).
17. G. Sauerbrey, Z. Phys., 178:457 (1964).
18. D. M. Ullevig, J. F. Evans, and M. G. Albrecht, Anal. Chem., 54:2341 (1982).
19. R. M. Mueller and W. White, Rev. Sci. Instr., 39:291 (1968).
20. D. King and G. R. Hoffman, J. Phys. E, 4:993 (1971).
21. see ref. 9, p. 3.
22. R. Schumacher, G. Borges, and K. K. Kanazawa, Surf. Sci., 163:L621 (1985).
23. R. Schumacher, J. G. Gordon, and O. Melroy, J. Electroanal. Chem., 216:127 (1987).
24. O. Melroy, K. K. Kanazawa, J. G. Gordon, and D. A. Buttry, Langmuir, 2:697 (1987).

25. M. Benje, M. Eiermann, U. Pittermann, and K. G. Weil, Ber. Bunsen - Ges. Phys. Chem., 90:435 (1986).
26. D. Orata and D. A. Buttry, J. Am. Chem. Soc., 109:3574 (1987).
27. W. Stöckel and R. Schumacher, Ber. Bunsen - Ges. Phys. Chem., 91:345 (1987).
28. M. R. Deakin and O. Melroy, J. Electroanal. Chem., 239:321 (1988).
29. C. K. Baker and J. R. Reynolds, J. Electroanal. Chem., 251:307 (1988).
30. B. Parzen, Design of Crystal and Other Harmonic Oscillators, Wiley-Interscience, New York (1983).
31. W. Stockel and R. Schumacher, Ber. Bunsen - Ges. Phys. Chem., 91:345 (1987).
32. M. D. Ward, J. Phys. Chem., 92:2049 (1988).
33. S. Gottesfeld, private communication.
34. R. Morrison, Grounding and Shielding Techniques in Instrumentation, Wiley Interscience, New York (1987).
35. J. G. Miller and D. I. Bolef, J. Appl. Phys., 39:5815 (1968).
36. C. Lu and O. Lewis, J. Appl. Phys., 43:4385 (1972).
37. E. Benes, J. Appl. Phys., 56:608 (1984).
38. A. P. M. Glassford, J. Vac. Sci. Technol., 15:1836 (1978).
39. K. K. Kanazawa and J. G. Gordon, Anal. Chim. Acta, 175:99 (1985).
40. K. K. Kanazawa and J. G. Gordon, Anal. Chem., 57:1770 (1985).
41. H. E. Hager, Chem. Eng. Commun., 43:25 (1986).
42. H. Muramatsu, E. Tamiya, and I. Karube, Anal. Chem., 60:2142 (1988).
43. J. D. Ferry, Viscoelastic Properties of Polymers, Wiley Interscience, New York, 1980.
44. C. E. Reed, K. K. Kanazawa, and J. F. Kaufman, preprint.
45. G. S. Ostrom and D. A. Buttry, J. Electroanal. Chem., 256:411 (1988).
46. S. Bruckenstein and M. Shay, J. Electroanal. Chem., 188:131 (1985).
47. M. R. Deakin, T. T. Li, and O. R. Melroy, J. Electroanal. Chem., 243:343 (1988).
48. S. Bruckenstein and S. Swathirajan, Electrochim. Acta, 30:851 (1985).
49. J. J. Donohue, L. J. Nordyke, and D. A. Buttry, Chemically Modified Surfaces in Science and Industry (D. E. Leyden and W. T. Collins, eds.), Gordon and Breach, New York, p. 377 (1988).

50. J. J. Donohue and D. A. Buttry, Langmuir, in press.
51. T. Saji, K. Hoshino, and A. Aoyagui, J. Am. Chem. Soc., 107:6865 (1985).
52. J. J. Donohue and D. A. Buttry, manuscript in preparation.
53. A. Grzegorzewski and K. E. Heusler, J. Electroanal. Chem., 228:455 (1987).
54. S. Bruckenstein and A. R. Hillman, J. Phys. Chem., 92:4837 (1988).
55. E. Mori, C. K. Baker, J. R. Reynolds, and K. Rajeshwar, J. Electroanal. Chem., 252:441 (1888).
56. R. W. Murray, Electroanalytical Chemistry (A. J. Bard, ed.), Marcel Dekker, New York, p. 191 (1984).
57. P. T. Varineau and D. A. Buttry, J. Phys. Chem., 91:1291 (1987).
58. P. T. Varineau and D. A. Buttry, manuscript in preparation.
59. see: S. Sinha, L. J. Ames, M. H. Schmidt, and A. B. Bocarsly, J. Electroanal. Chem., 210:323 (1986) and references therein.
60. S. J. Lasky and D. A. Buttry, J. Am. Chem. Soc., 110:6258 (1988).
61. B. J. Feldman and O. R. Melroy, J. Electroanal. Chem., 234:213 (1987).
62. see: R. M. Penner and C. R. Martin, J. Phys. Chem., 92:5274 (1988) and references therein.
63. J. R. Reynolds, N. S. Sundaresan, M. Pomerantz, S. Basak, and C. K. Baker, J. Electroanal. Chem., 250:355 (1988).
64. J. N. Kaufman, K. K. Kanazawa, and G. B. Street, Phys. Rev. Lett., 53:2461 (1984).
65. D. Orata and D. A. Buttry, J. Electroanal. Chem., 257:71 (1988).
66. J. M. Saveant, J. Phys. Chem., 92:4526 (1988).
67. H. E. Hager, G. A. Escobar, and P. D. Verge, J. Appl. Phys., 59:3328 (1986).

Apparent MW's of the deposit formed for various applied potentials.

Table 1<sup>a</sup>

Concentration of DHVBr <sub>2</sub> (mM)	Concentration of KBr (M)	Final Potential (V)	MW (g/mole)
1	0.3	-0.580	866
1	0.3	-0.600	731
1	0.3	-0.750	449
<hr/>			
5	0.3	-0.535	1205
5	0.3	-0.536	1145
5	0.3	-0.537	957
5	0.3	-0.538	926
5	0.3	-0.750	460

<sup>a</sup>From Ref. 45, with permission.

## Figure Captions

1. Edge view of QCM disk showing shear deformation. The disk thickness and shear deformation have been exaggerated for clarity.
2. Top view of QCM disk with vapor deposited electrodes. Disk diameter - 1 inch. Area of central circular pad -  $0.28 \text{ cm}^2$ . Width of rectangular flag for external connection - 2 mm. The thin film metal electrodes are ca. 300 nm thick.
3. Schematic of oscillator circuit. IC1 - MC1733. R1 -  $2.2 \text{ M}\Omega$ . R2 -  $200 \Omega$ . R3, R4, R5, R6 -  $180 \Omega$ . R7 -  $220 \Omega$ . C1 -  $0.01 \mu\text{F}$ . T1, T2 - 2N3904. D1, D2 - HP 5082-2811 Schottky diodes.
4. Schematic of EQCM apparatus.
5. a) Equivalent circuit representing the electrical behavior of a QCM. b) Equivalent representation of the circuit in (a).
6. Shear velocity profiles in a fluid adjacent to a QCM at three different times: a) peak surface velocity, b) intermediate surface velocity, c) zero surface velocity. (From Ref. 40, with permission.)
7. Plots of conductance versus relative frequency for a 5 MHz AT-cut QCM of the type shown in Figure 2 in a) air, b) water. The scale for curve b has been increased by 5x.
8. Schematic depiction of pit nucleation and growth during thin film dissolution.

9. UPD of Bi (1.0 mM in 0.1 M HClO<sub>4</sub>) on Au at 10 mV s<sup>-1</sup>, average of 30 scans, background corrected. The current response of the EQCM Au electrode (dashed) and the derivative representation of d(Δf)/dE versus E from equation 20 (solid), assuming  $\gamma = 3$ . (From Ref. 28, with permission.)

10. a) CV scan for 22 μM C12. b) EQCM frequency response for scan in (a). Scan rate - 50 mV s<sup>-1</sup>. Supporting electrolyte - 1.0 M H<sub>3</sub>PO<sub>4</sub>. The data have been digitally smoothed using a fourier filter and background corrected. (From Ref. 50, with permission.)

11. a) CV scan for 0.5 mM C12. b) EQCM frequency response for scan in (a). Scan rate - 50 mV s<sup>-1</sup>. Supporting electrolyte - 0.2 M Li<sub>2</sub>SO<sub>4</sub>, adjusted to pH 3 with 0.2 M H<sub>2</sub>SO<sub>4</sub>. The CV has been treated as in Figure 10. (From Ref. 49, with permission.)

12. a) CV scan of 15 μM C16. Scan rate - 50 mV s<sup>-1</sup>. b) EQCM frequency response for the scan in (a). Scan rates - (A) 250 mV s<sup>-1</sup>. (B) 50 mV s<sup>-1</sup>. (C) 10 mV s<sup>-1</sup>. Supporting electrolyte - 1.0 M H<sub>2</sub>SO<sub>4</sub>.

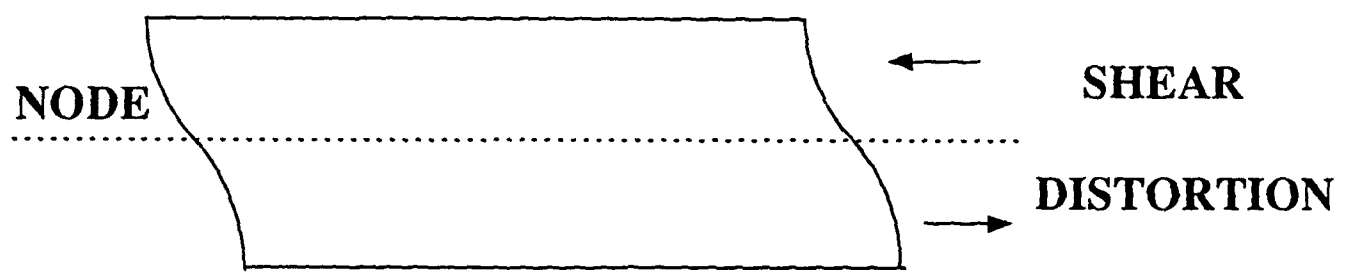
13. a) Relative frequency change versus time for a 10 second step from +0.2 to -0.75 (i.e. over the first reduction wave) for a solution containing 5 mM DHVBr<sub>2</sub>, 0.3 M KBr, and 5 mM NaOH. b) Plot of relative frequency change versus the square root of time for the data in (a). (From Ref. 45, with permission.)

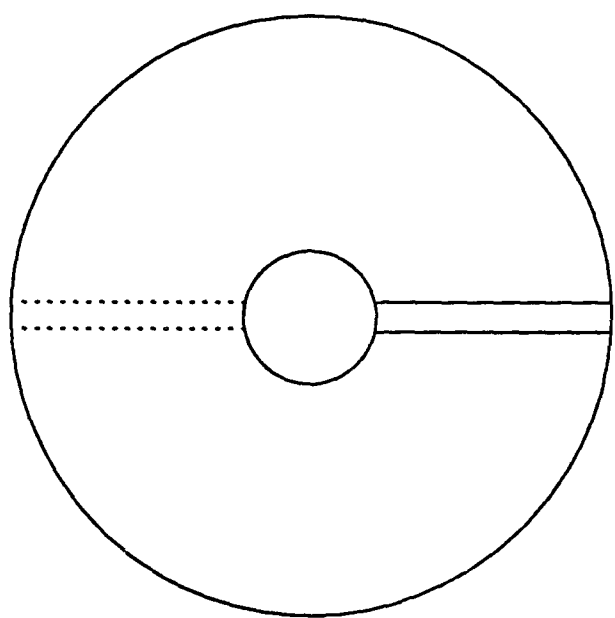
14. Schematic depiction of solution "trapping" between nuclei during the nucleation stage of a deposition.

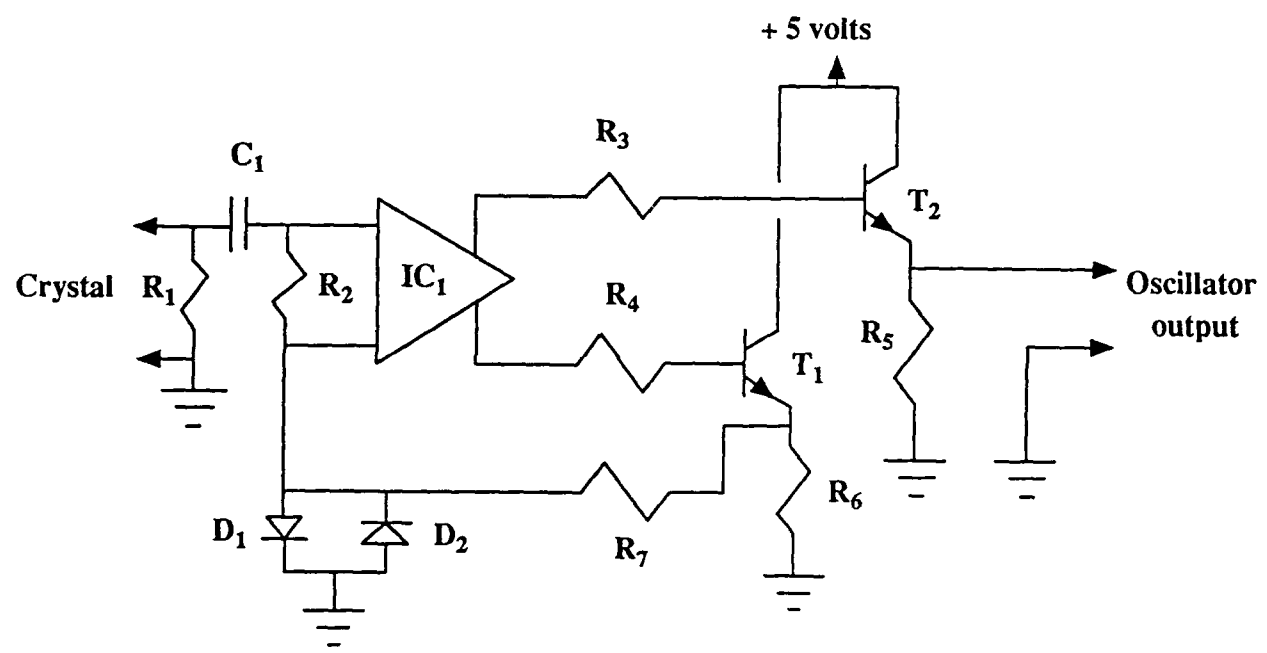
15. a) CV of PVF in 0.1 M KPF<sub>6</sub>. Scan rate - 10 mV s<sup>-1</sup>. b) EQCM frequency response for the scan in (a). (From Ref. 57, with permission.)

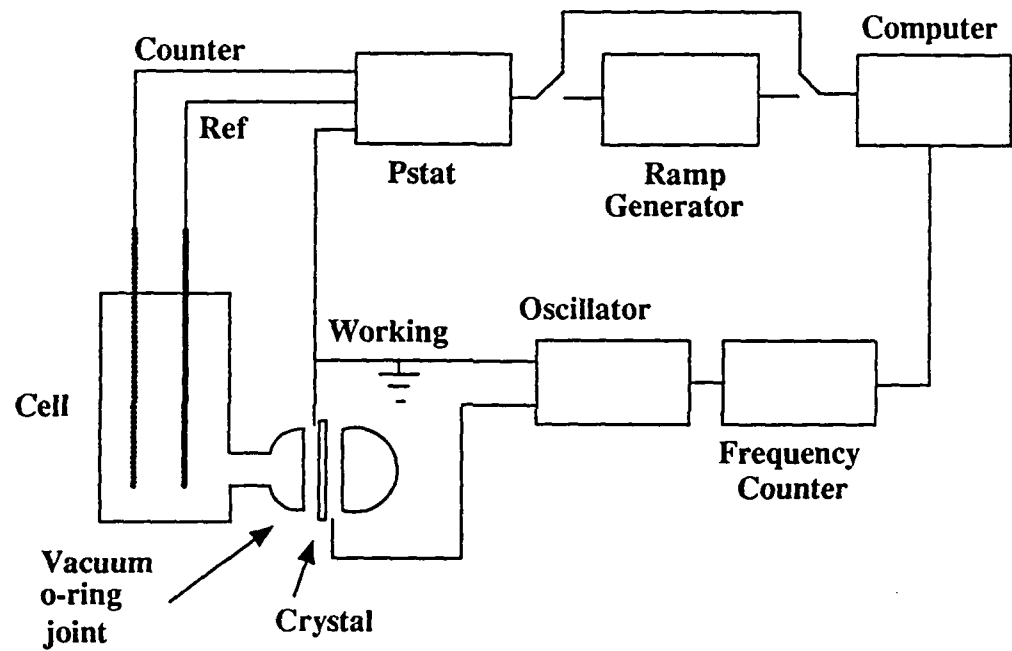
16. a) CV of PVF in 0.1 M KIO<sub>3</sub>. Scan rate - 50 mV s<sup>-1</sup>. b) d(Δf)/dE versus E (from equation 20) for the scan in (a).
17. a) CV of PVF in 1.0 M NaCl. Scan rate - 50 mV s<sup>-1</sup>. b) EQCM frequency response for the scan in (a). (From Ref. 57, with permission.)
18. A. a) CV of a nickel ferrocyanide film in 0.1 M CsCl/H<sub>2</sub>O. Scan rate - 100 mV s<sup>-1</sup>. b) Same as in (a) except that the solution contains D<sub>2</sub>O rather than H<sub>2</sub>O. B. a) EQCM frequency response for the scan in (a). b) Same for (b). (From Ref. 60, with permission.)
19. Schematic representation of the frequency changes measured and calculated for the CV's in Figure 18. (From Ref. 60, with permission.)
20. a) CV scan during the electropolymerization of PA in 0.1 M aniline, 1.0 M H<sub>2</sub>SO<sub>4</sub>. Scan rate - 100 mV s<sup>-1</sup>. C = 100 μA. b) EQCM frequency response for the scan in (a). F = 20 Hz. Curve (b) is offset 40 mV to the left with respect to curve (a). (From Ref. 26, with permission.)
21. Schematic depiction of cation transport during switching in a PA/Nafion composite film.
22. a) CV scan during electropolymerization of PA in a Nafion film in 0.1 M aniline, 1.0 M H<sub>2</sub>SO<sub>4</sub>. Scan rate - 200 mV s<sup>-1</sup>. C = 20 μA. b) EQCM frequency response for the scan in (a). F = 10 Hz. (From Ref. 65, with permission.)
23. a) CV scan of PA/Nafion composite film in 0.1 M CsCl. Scan rate - 200 mV s<sup>-1</sup>. C =

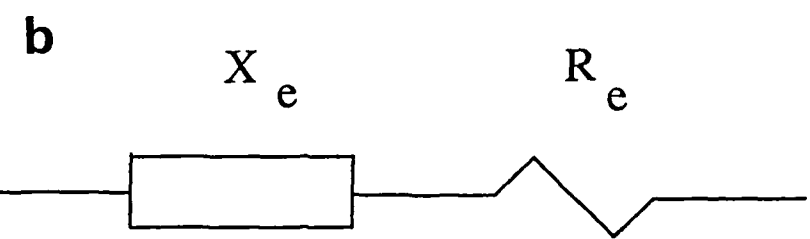
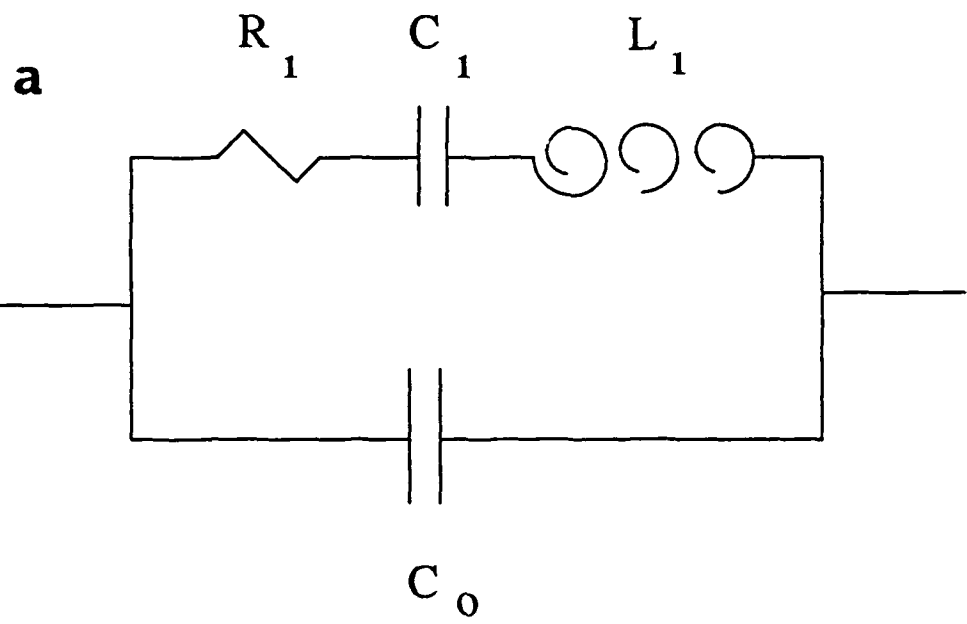
20  $\mu$ A. b) EQCM frequency response for scan in (a).  $F = 5$  Hz. (From Ref. 65, with permission.)

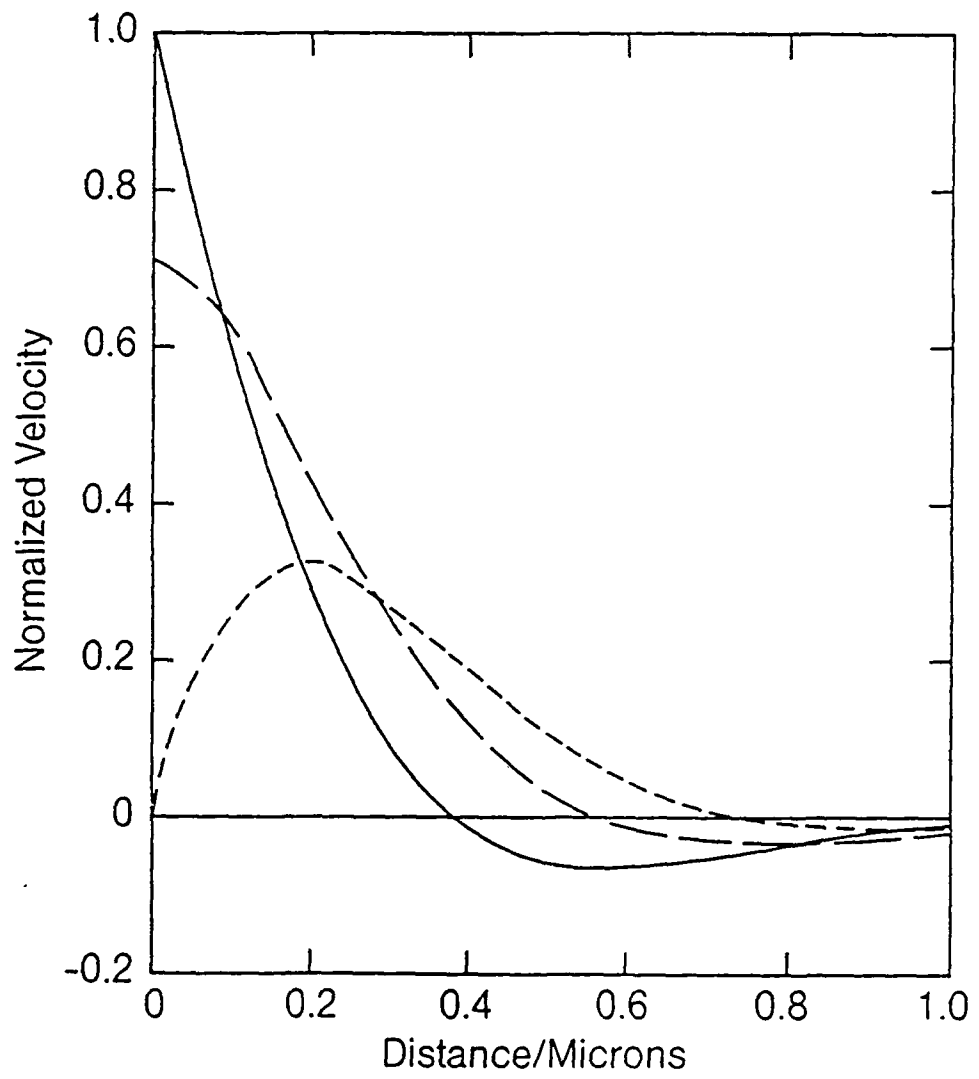


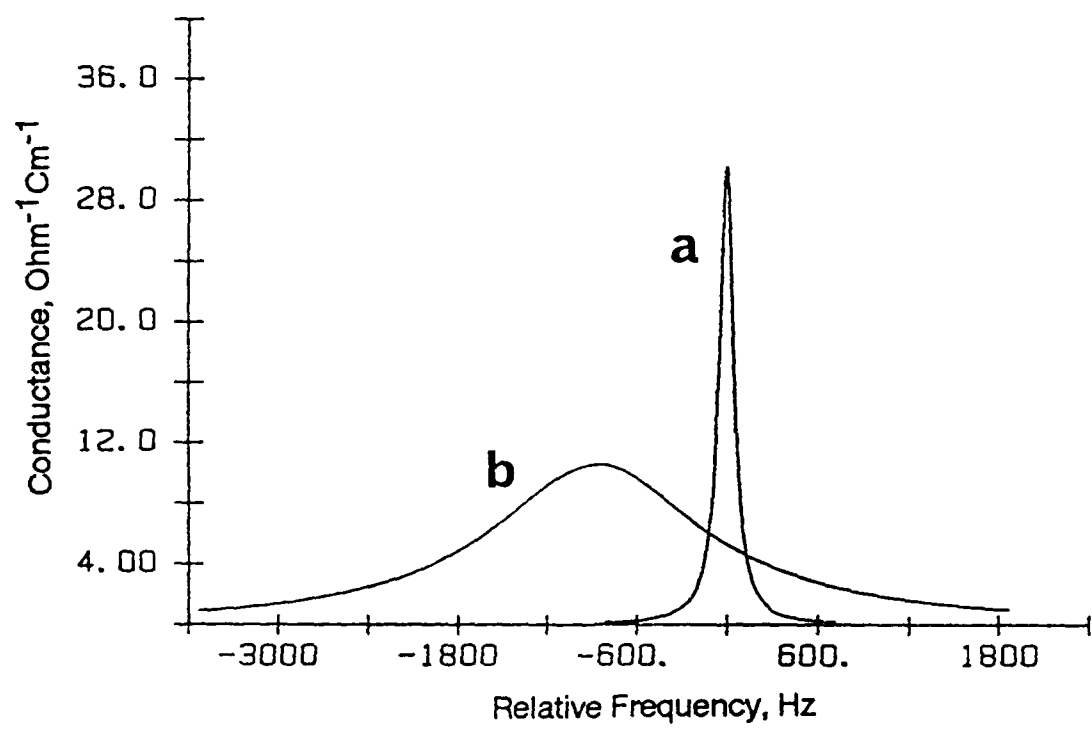


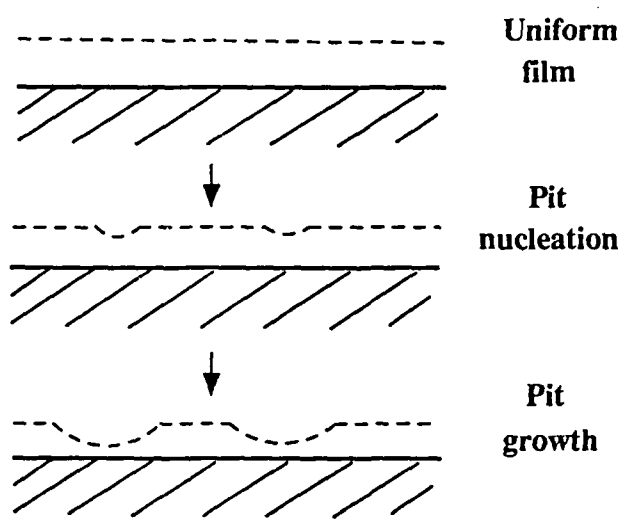


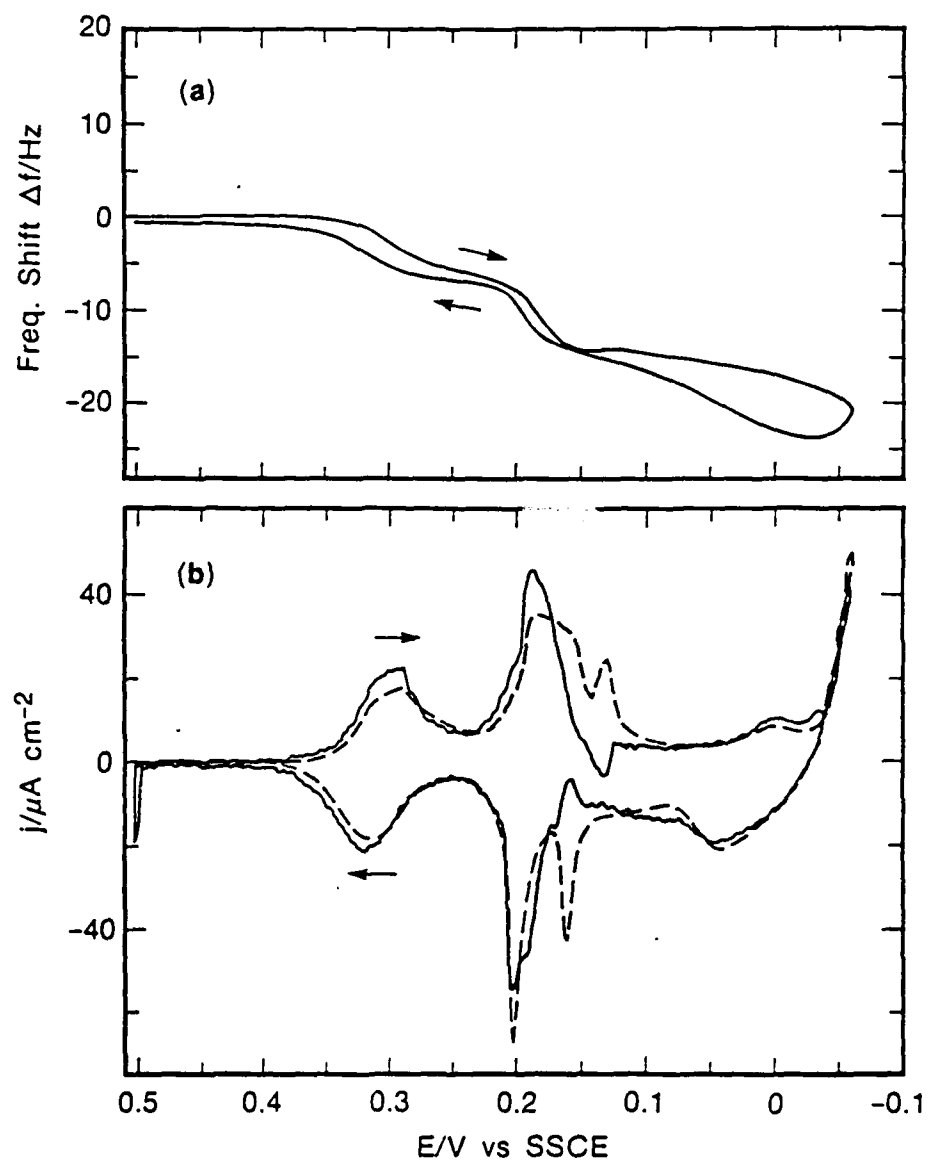


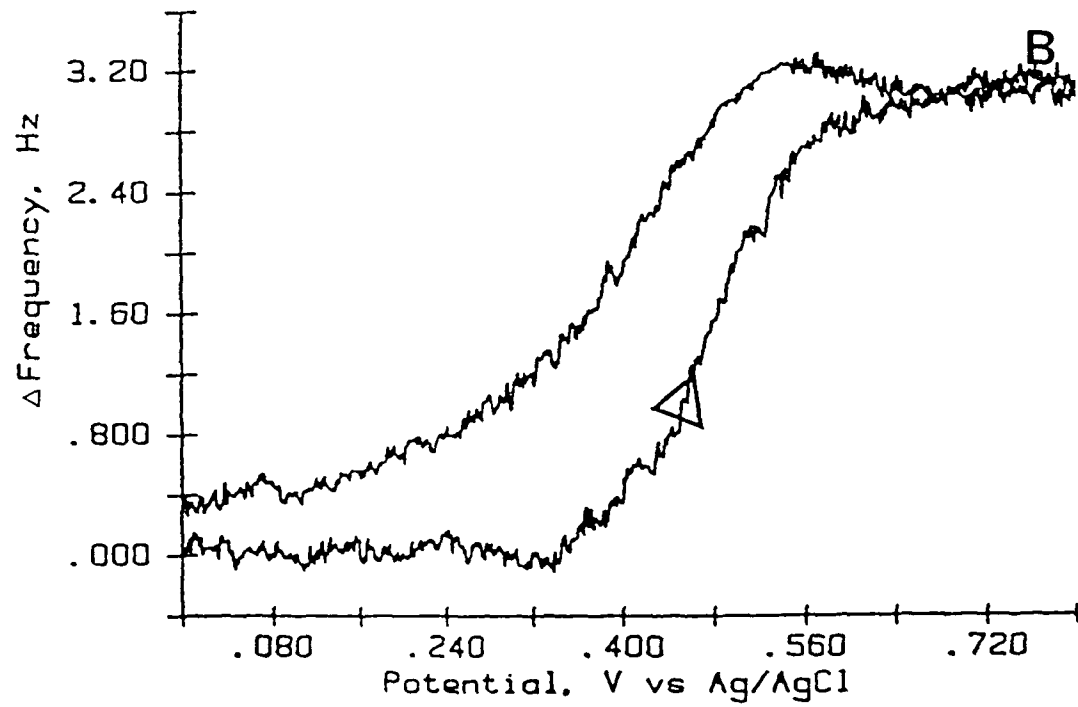
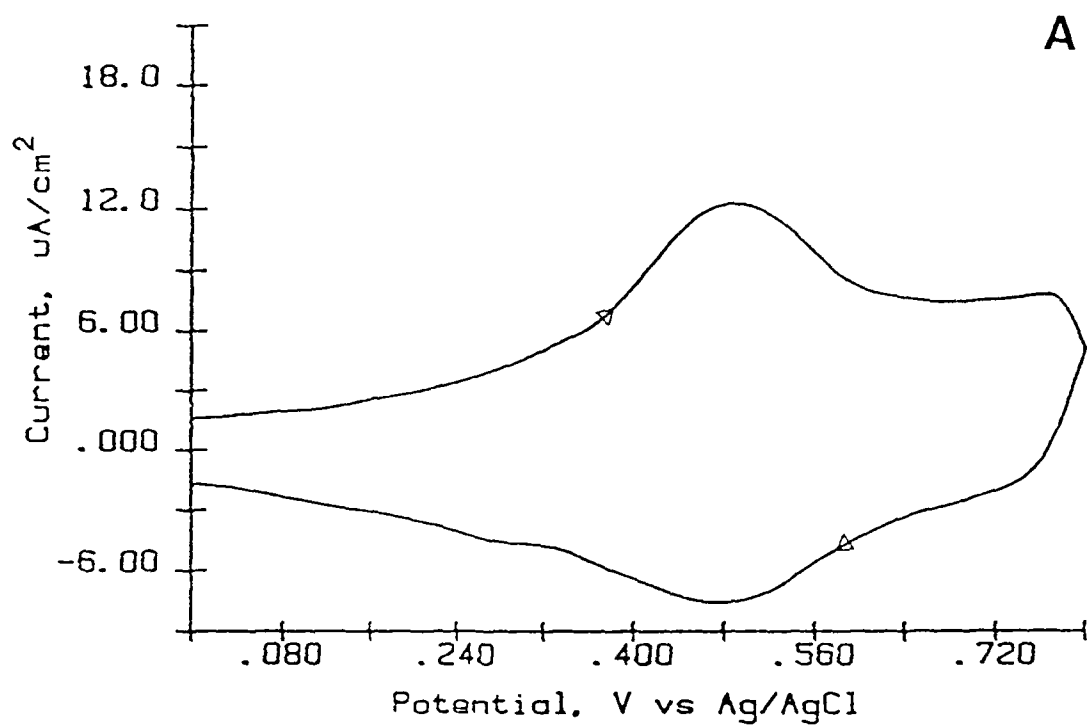


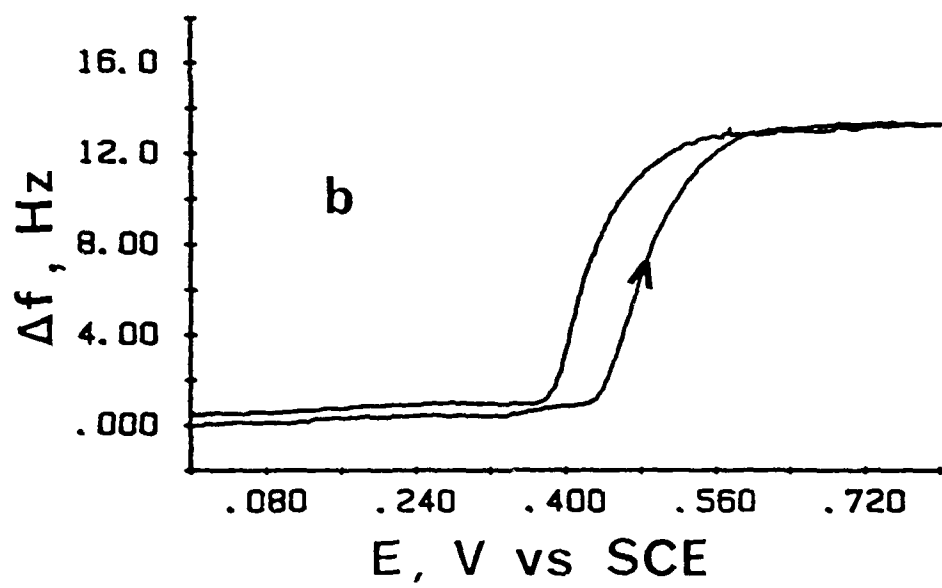
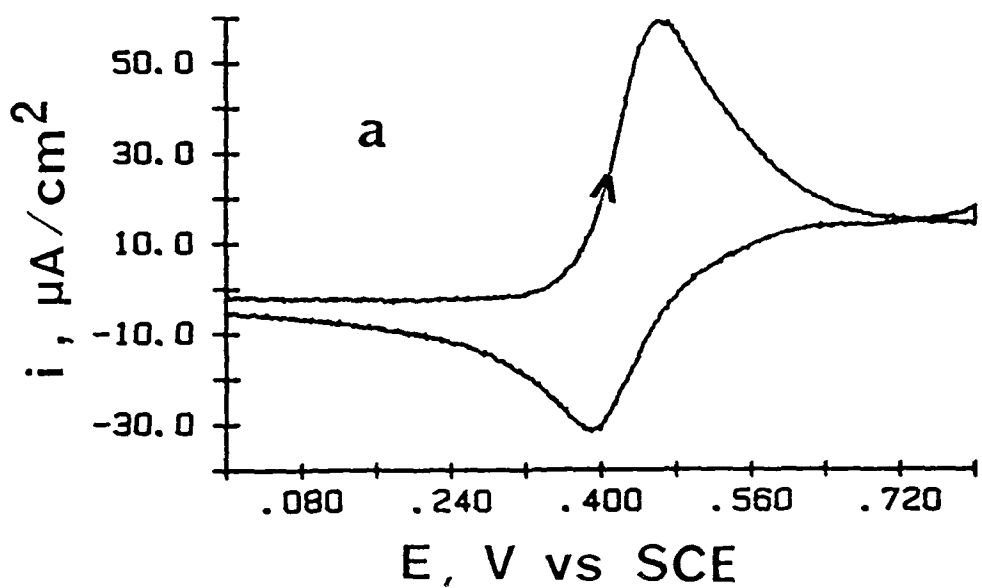


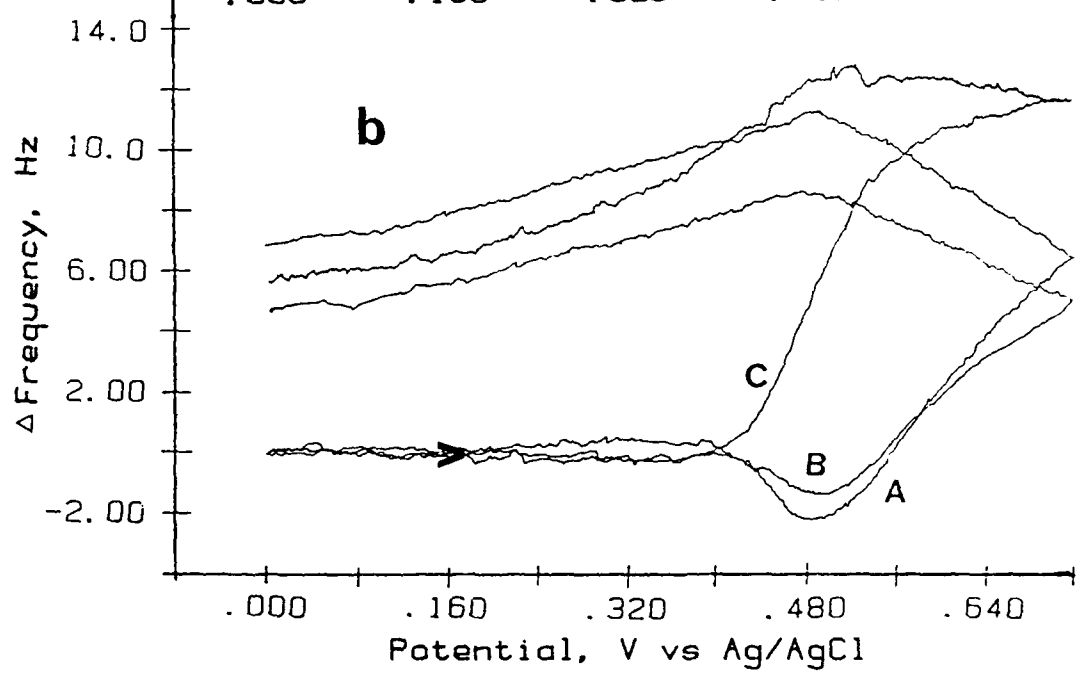
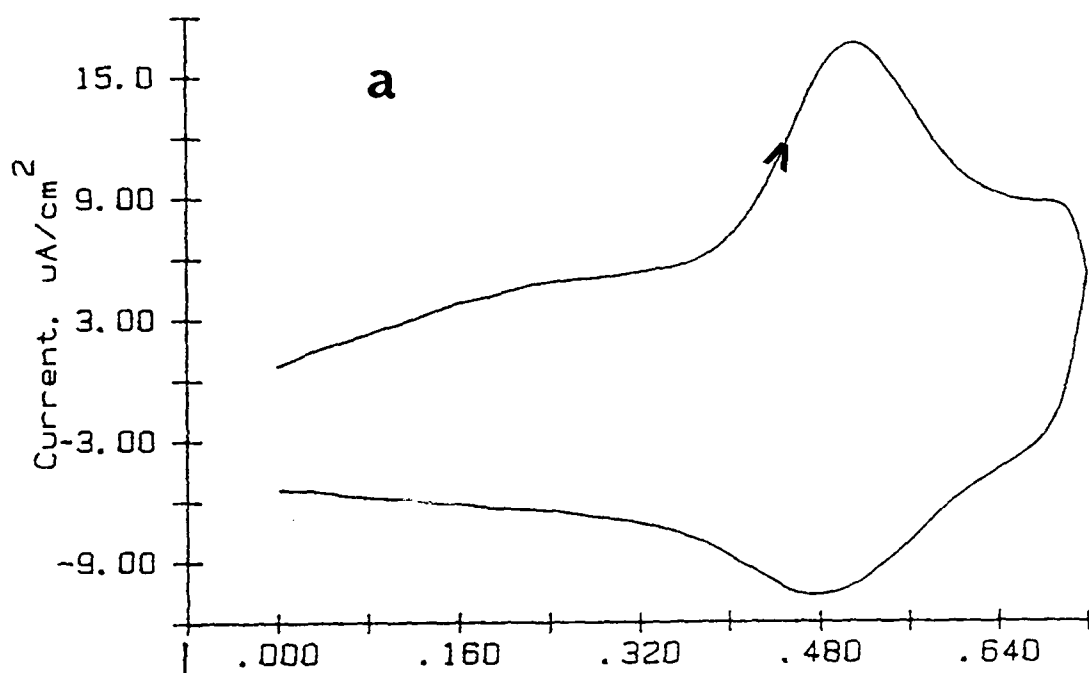


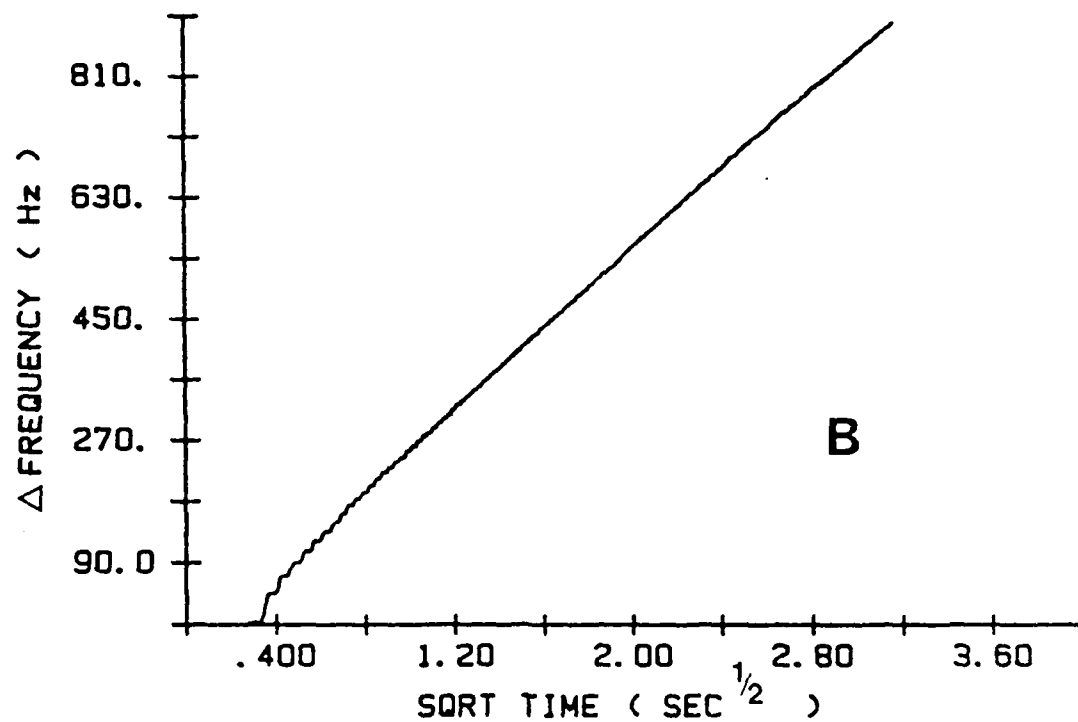
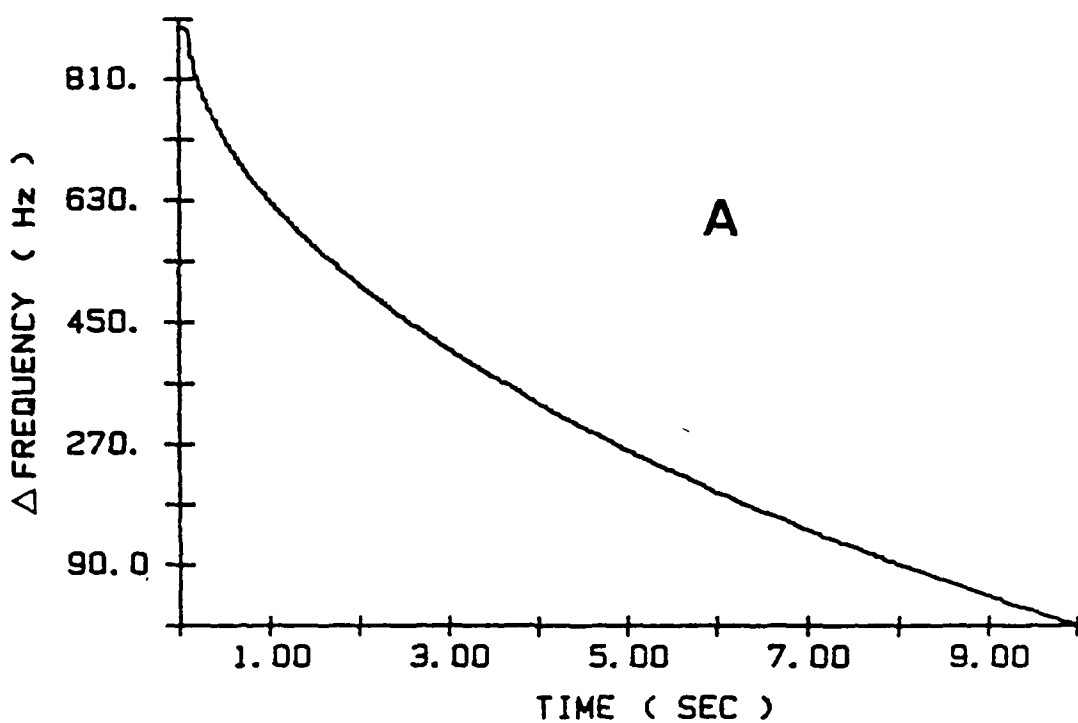












**Solution "trapped"  
between nuclei**

